

KEK-TH-1134

YITP-07-03

The study of $\tilde{q}_L\tilde{q}_L$ production at LHC in the $l^\pm l^\pm$ channel and sensitivity to other models

Mihoko M.Nojiri* and Michihisa Takeuchi†

*† *Theory Group, KEK,*

and **the Graduate University for Advanced Studies (SOKENDAI)*

1-1 *Oho, Tsukuba, 305-0801, Japan*

† *Yukawa Institute for Theoretical Physics,*

Kyoto University,

Kyoto 606-8502, Japan

(Dated: December 24, 2018)

Abstract

At LHC, $\tilde{q}_L\tilde{q}_L$ production is one of main SUSY production processes in the MSSM, which occurs due to the chirality flip caused by Majorana gluino mass. The process is one of the sources of same sign two lepton (SS2l) events, however, gluino production also contribute to the channel. In this paper, we develop a method to identify gluino and squark production separately for the SS2l channel, based on the cuts on the kinematical configuration of the jets. We applied the method to the MSSM, the model with an extended gluino sector, the Little Higgs model with T-parity (LHT), and found the distinctive difference between the models using the numbers of SS2l events under the cuts.

*Electronic address: nojiri@post.kek.jp

†Electronic address: tmichihi@post.kek.jp

I. INTRODUCTION

The Standard Model (SM) describes interactions among elementary particles very well. But astrophysical and cosmological observations such as WMAP have confirmed the existence of the dark matter (DM) that cannot be explained in the SM [1]. The particle which consists of DM does not leave detectable signal in the detectors at high energy collider experiments, because it should be weakly interacting.

If new particles are produced at collider experiments and decay into visible particles and a DM particle, we can observe large missing transverse momentum (\cancel{E}_T) in the events. Many models which predict DM candidates have been proposed. Among them, the minimal supersymmetric standard model with conserved R-parity (MSSM) is attractive one. The lightest supersymmetric particle (LSP) is stable and a DM candidate. In the MSSM, quadratic divergences in the Higgs mass radiative corrections cancel each other, therefore the fine tuning problem is solved. At large hadron collider (LHC), which is pp collider with $\sqrt{s} = 14$ TeV starting its operation in 2007 [2, 3], discovery of the squarks \tilde{q} and gluino \tilde{g} – super partners of quarks and gluon – is possible for the masses up to 2.5 TeV by looking for the excess of the events with large \cancel{E}_T . We can also measure the mass spectrum of them by studying the decay kinematics of the quarks and gluino decay chains if there is enough statistics.

However, the discovery of \cancel{E}_T signature does not necessarily mean the confirmation of the existence of supersymmetry. Similar mass spectrum and decay pattern might be obtained for the Universal Extra Dimension model (UED) [4] and the Littlest Higgs model with T parity (LHT) [5]. To study the origin of the \cancel{E}_T signature, therefore, it is important to measure the other features that are characteristic for the MSSM.

Many analyses have already been carried out in this direction. Recently, the processes sensitive to the $\tilde{g}\tilde{q}q$ Yukawa type coupling constant has been investigated in [6]. The Yukawa type coupling constant for $\tilde{g}\tilde{q}q$ vertex is the same as the gauge coupling constant due to the SUSY. They study same sign two isolated-lepton (SS2l) channel for estimating the production cross section $\sigma(\tilde{q}_L\tilde{q}_L)$. The process is in principle sensitive to the coupling, but, they found the large background from $\tilde{g}\tilde{q}$ production. To measure the coupling constant, it is important to measure the cross sections of sparticle production processes separately. In this paper, we also focus on the $\sigma(\tilde{q}_L\tilde{q}_L)$. We will give the new method based on cuts on the numbers of jets in the hemispheres for the purpose of separating the $\tilde{q}_L\tilde{q}_L$ production from

$\tilde{g}\tilde{q}_L$ production.

The $\tilde{q}_L\tilde{q}_L$ production process occurs through the chirality flip caused by gluino majorana mass term $m_g\tilde{g}\tilde{g}$. To study the sensitivity to the majorana nature of the gluino mass, we consider a model with an extended gluino sector. This extension is inspired by the model that extends SUSY to $N = 2$ in [7, 8, 9, 10]. In this model, an adjoint matter \tilde{a} is introduced, then gluino can have a Dirac mass term $m_D\tilde{g}\tilde{a}$. The gluino mass receives a contribution from m_D . We also discuss the Littlest Higgs model with T-parity (LHT). The model contains quark partners (q_-) and gauge boson partners (W_H, A_H) which decay into the stable lightest T-odd particle (LTP) A_H and SM particles as in the MSSM.

This paper is organized as follows. In Section 2, we first discuss the mass dependencies of the production cross section of \tilde{q} and \tilde{g} in the MSSM. The $\tilde{u}_L\tilde{u}_L$ production cross section is typically of the order of 100 fb at $m_{\tilde{q}} \sim m_{\tilde{g}} \sim 1$ TeV, which may be detectable at LHC. The production processes of $\tilde{q}_L\tilde{q}_L$ and $\tilde{q}_R\tilde{q}_R$ occur due to the gluino majorana mass, therefore the mass dependencies are different from those of $\sigma(\tilde{q}_L\tilde{q}_R)$ and $\sigma(\tilde{q}_L\tilde{q}_L^*)$. We compare $\sigma(\tilde{q}_L\tilde{q}_L)$ with $\sigma(\tilde{g}\tilde{q}_L)$ and find out $\sigma(\tilde{q}_L\tilde{q}_L) \ll \sigma(\tilde{g}\tilde{q}_L)$. In this section, we also choose a few model points for later analyses.

For the MSSM with an extended gluino sector, the \tilde{g}, \tilde{q} production cross sections are the functions of the three mass parameters – two majorana masses m_g, m_A and one Dirac mass m_D , where the mass terms are of the form $m_g\tilde{g}\tilde{g} + m_A\tilde{a}\tilde{a} + m_D(\tilde{a}\tilde{g} + \tilde{g}\tilde{a})$. Especially, the $\sigma(\tilde{q}_L\tilde{q}_L)$ becomes zero for some particular choice of parameters. We also discuss the LHT model. The production process q_-q_- occurs by the heavy SU(2) gauge boson exchanges. The $\sigma(q_-q_-)$ is large compared with $\sigma(\tilde{q}\tilde{q})$ of the MSSM [11]. On the other hand, because no gluon partner exists in this model, there is no problematic background corresponding to $\tilde{g}\tilde{q}$ productions of the MSSM.

In Section 3, We study SS2l events to estimate $\sigma(\tilde{q}_L\tilde{q}_L)$ in the MSSM. To reduce SS2l events from $\tilde{g}\tilde{q}_L$, we use b -jet veto and the numbers of jets in hemispheres defined following the procedure proposed in [12]. We demonstrate that production processes $\tilde{g}\tilde{g}, \tilde{g}\tilde{q}, \tilde{q}\tilde{q}$ can be distinguished by the efficiency under the cuts. We also discuss the dominant $t\bar{t}$ background.

In Section 4, we calculate the expected number of SS2l events in the model with an extended gluino sector considered in Section 2. We discuss the sensitivity of the $\tilde{q}_L\tilde{q}_L$ production cross section to the majorana gluino mass m_g at a few model points. We also estimate the number of SS2l signature in the LHT model. The efficiency under the cuts

to reduce gluino background turns out to be useful to prove the existence of quark partner productions and difference from the MSSM prediction. Section 5 is devoted to the summary.

II. PRODUCTION CROSS SECTIONS AT LHC

A. MSSM production cross sections at LHC

In the MSSM, sparticles are always pair produced at LHC because of R-parity conservation. Production processes $\tilde{g}\tilde{g}$, $\tilde{g}\tilde{q}$, $\tilde{q}\tilde{q}$ occur copiously unless the masses are much heavier than 1 TeV. Because u quark and d quark parton distribution functions (PDF) of a proton are much harder than the other partons, \tilde{u} and \tilde{d} are mainly produced among squarks. Especially, production processes $\tilde{u}_L\tilde{u}_L$, $\tilde{d}_L\tilde{d}_L$, $\tilde{u}_R\tilde{u}_R$, $\tilde{d}_R\tilde{d}_R$, etc. require chirality flip, therefore they do not occur if the gluino mass is not a majorana type $m_g\lambda\lambda$. Only gluino exchange diagrams contribute to the productions.¹

If the sparticle mass spectrum is known, the production cross sections at LHC are calculable. The mass dependencies of some sparticle production cross sections are shown in Figure 1~3. Here, we use CTEQ 6l [13] for PDF. The horizontal axis is the gluino mass $m_{\tilde{g}}$, and the vertical axis is the squark mass $m_{\tilde{q}}$.² The production cross section of each process is shown in contour lines in the unit of pb.

The $\sigma(\tilde{q}_L\tilde{q}_L)$ ($\tilde{q}_L = \tilde{u}_L$ or \tilde{d}_L) are shown in Figure 1 a ~ c. The $\sigma(\tilde{u}_L\tilde{u}_L)$ is 0.05 pb at $m_{\tilde{q}} = m_{\tilde{g}} = 1000$ GeV, and 0.12 pb at $m_{\tilde{q}} = m_{\tilde{g}} = 800$ GeV. This shows that they strongly depend on the squark mass $m_{\tilde{q}}$. The mass measurement error at LHC for squarks and gluino can be around a few percent, if the statistics are enough [14]. The $\sigma(\tilde{q}_L\tilde{q}_L)$ changes 10% when $m_{\tilde{q}}$ changes 3% around $m_{\tilde{q}} = m_{\tilde{g}} = 1000$ GeV and $m_{\tilde{q}} = m_{\tilde{g}} = 800$ GeV. On the other hand, the cross section only weakly depends on gluino mass. This is because the amplitude has factor of $m_{\tilde{g}}$ from chirality flip, which compensates the suppression from the t-channel propagator. The $\sigma(\tilde{u}_L\tilde{u}_L)$ changes within 10% in the range $500 \text{ GeV} < m_{\tilde{g}} < 1100 \text{ GeV}$ around $m_{\tilde{q}} = 800$ GeV, and also changes within 10% in the range $700 \text{ GeV} < m_{\tilde{g}} < 1300 \text{ GeV}$ around $m_{\tilde{q}} = 1000$ GeV (Figure 1a). In case of $m_{\tilde{g}} = 3$ TeV, $\sigma(\tilde{u}_L\tilde{u}_L)$ is 0.04 pb at $m_{\tilde{q}} =$

¹ Here, we neglect the contributions from neutralino and chargino exchange diagrams. This assumption is reasonable, because the $g^2 < g_s^2, m_{\tilde{W}} < m_{\tilde{g}}$ in mSUGRA.

² We set $m_{\tilde{u}_L} = m_{\tilde{q}}$, $m_{\tilde{d}_L} = m_{\tilde{q}} + 6$ GeV, $m_{\tilde{u}_R} = m_{\tilde{q}} - 19$ GeV.

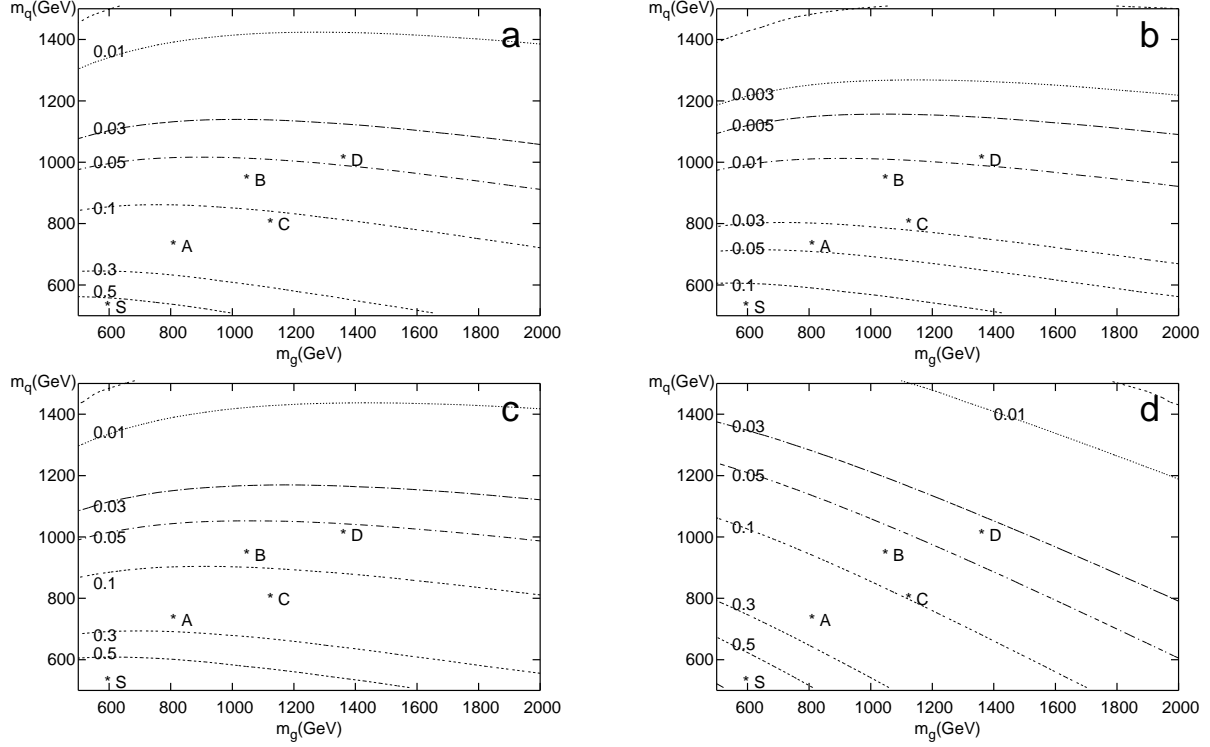


FIG. 1: Contour plot of a) $\sigma(\tilde{u}_L \tilde{u}_L)$, b) $\sigma(\tilde{d}_L \tilde{d}_L)$, c) $\sigma(\tilde{u}_L \tilde{d}_L)$ and d) $\sigma(\tilde{u}_L \tilde{u}_R)$ as the function of $m_{\tilde{g}}$ and $m_{\tilde{q}}$.

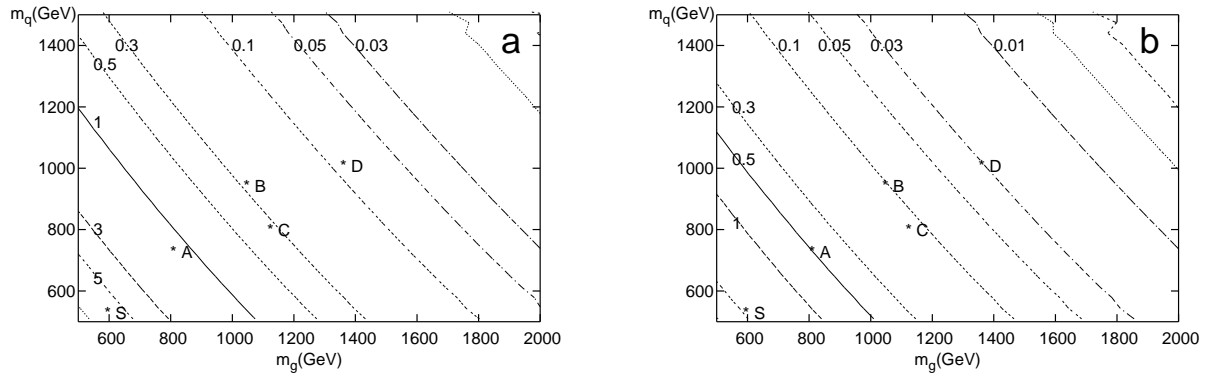


FIG. 2: Contour plot of a) $\sigma(\tilde{g} \tilde{u}_L)$ and b) $\sigma(\tilde{g} \tilde{d}_L)$ as the function of $m_{\tilde{g}}$ and $m_{\tilde{q}}$.

800 GeV, and 0.02 pb at $m_{\tilde{q}} = 1000$ GeV. As a result, even when the accuracy of the mass measurement of gluino is bad, the $\tilde{q}_L \tilde{q}_L$ production cross section is useful observable that can be used to test the MSSM quantitatively. The behavior of the $\tilde{q}_R \tilde{q}_R$ production cross section is the same.

The $\sigma(\tilde{q}_L \tilde{q}_R)$ (such as $\sigma(\tilde{u}_L \tilde{u}_R)$ etc.) depends on the gluino mass more sensitively than $\sigma(\tilde{q}_L \tilde{q}_L)$. It decreases as the gluino mass increases. The $\sigma(\tilde{u}_L \tilde{u}_R)$ drops by half as $m_{\tilde{g}}$

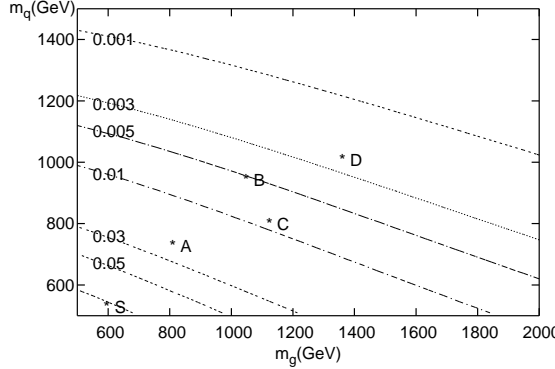


FIG. 3: Contour plot of $\sigma(\tilde{u}_L \tilde{d}_L^*)$ as the function of $m_{\tilde{g}}$ and $m_{\tilde{q}}$.

increases 500 GeV to 1100 GeV for $m_{\tilde{q}} = 800$ GeV, and also drops by half as $m_{\tilde{g}}$ increases 700 GeV to 1300 GeV for $m_{\tilde{q}} = 1000$ GeV (Figure 1d). The $\sigma(\tilde{g}\tilde{q}_L)$ depends on the gluino mass further more because an onshell gluino has to be produced (Figure 2a,2b).

By investigating $\tilde{q}_L \tilde{q}_L$ production processes, we can probe the majorana nature of gluino mass. To measure the production cross section of $\tilde{u}_L \tilde{u}_L$, $\tilde{d}_L \tilde{d}_L$, same sign two lepton (SS2l) events are useful, which is studied in [6]. This idea is as follows; a $\tilde{u}_L(\tilde{d}_L)$ may dominantly produces $l^+(l^-)$ thorough the decays of

$$\begin{aligned} \tilde{u}_L \rightarrow \tilde{\chi}_1^+ d \rightarrow \tilde{l}^+ \nu_l d \rightarrow \tilde{\chi}_1^0 l^+ \nu_l d & \quad \tilde{d}_L \rightarrow \tilde{\chi}_1^- u \rightarrow \tilde{l}^- \bar{\nu}_l u \rightarrow \tilde{\chi}_1^0 l^- \bar{\nu}_l u \\ \text{or } \rightarrow \tilde{\chi}_1^0 W^+ d \rightarrow \tilde{\chi}_1^0 l^+ \nu_l d, & \quad \text{or } \rightarrow \tilde{\chi}_1^0 W^- u \rightarrow \tilde{\chi}_1^0 l^- \bar{\nu}_l u. \end{aligned} \quad (1)$$

Therefore l^+l^+ events are sensitive to the $\tilde{u}_L \tilde{u}_L$ production and l^-l^- events to $\tilde{d}_L \tilde{d}_L$ production. This signature implies the existence of the Yukawa type vertex $g\tilde{g}\tilde{q}$.

The ratio of l^+l^+ and l^-l^- has more information. The ratio of fractions of u and d in PDF are 2:1. Then, the $\sigma(\tilde{u}_L \tilde{u}_L)$ is larger than $\sigma(\tilde{d}_L \tilde{d}_L)$ and their ratio is about 4:1 (Figure 1a,b). Thus the ratio of the number of SS2l events $N(l^+l^+ \text{ from } \tilde{u}_L \tilde{u}_L) : N(l^-l^- \text{ from } \tilde{d}_L \tilde{d}_L)$ should be 4:1 if leptonic branching ratios of \tilde{u}_L and \tilde{d}_L are the same.

The processes involving \tilde{u}_L^* and \tilde{d}_L^* etc. also become the sources of SS2l events although the cross section is not large ($\sigma(\tilde{u}_L \tilde{d}_L^*) \sim 0.1\sigma(\tilde{u}_L \tilde{u}_L)$ in Figure 3). Since the basic observable is the sign of leptons, in the following we define \tilde{q}_L^+ as $\{\tilde{u}_L, \tilde{d}_L^*, \tilde{c}_L, \tilde{s}_L^*\}$ which can be a parent of l^+ , and \tilde{q}_L^- as $\{\tilde{u}_L^*, \tilde{d}_L, \tilde{c}_L^*, \tilde{s}_L\}$ which can be a parent of l^- .

The mass dependencies of the production cross sections of \tilde{q}_L^+ , \tilde{q}_L^- are calculated in Figure 4~6. By comparing Figure 4a with Figure 1a, and Figure 4b with Figure 1b, we can see that $\tilde{u}_L \tilde{u}_L$ ($\tilde{d}_L \tilde{d}_L$) is dominant in $\tilde{q}_L^+ \tilde{q}_L^+$ ($\tilde{q}_L^- \tilde{q}_L^-$) respectively. By comparing Figure 5a with

Figure 2a, and Figure 5b with Figure 2b, we also find that $\tilde{g}\tilde{u}_L$ ($\tilde{g}\tilde{d}_L$), is dominant in $\tilde{g}\tilde{q}_L^+$ ($\tilde{g}\tilde{q}_L^-$) respectively.

The \tilde{g} can decay into $\tilde{q}_L^\pm q^\mp$, therefore $\tilde{g}\tilde{q}_L^\pm$ production also produce $l^\pm l^\pm$. Moreover, $\sigma(\tilde{g}\tilde{q}_L^\pm)$ is larger than $\sigma(\tilde{q}_L^\pm\tilde{q}_L^\pm)$ unless gluino is too heavy (Typically $\sigma(\tilde{g}\tilde{q}^\pm) \sim 5\sigma(\tilde{q}^\pm\tilde{q}^\pm)$), thus the $\tilde{g}\tilde{q}_L^\pm$ production process becomes background to the $\tilde{q}_L^\pm\tilde{q}_L^\pm$ production process. The ratio $\sigma(\tilde{g}\tilde{q}^+) : \sigma(\tilde{g}\tilde{q}^-)$ is about 2:1 (Figure 5). Then the ratio of the number of the SS2l events $N(l^+l^+ \text{ from } \tilde{g}\tilde{q}^+) : N(l^-l^- \text{ from } \tilde{g}\tilde{q}^-)$ should be 2:1.

The $\tilde{g}\tilde{g}$ production process also produces $l^\pm l^\pm$ and $N(l^+l^+ \text{ from } \tilde{g}\tilde{g}) : N(l^-l^- \text{ from } \tilde{g}\tilde{g})$ should be 1:1. This process, however, does not produce problematic background because the SS2l branching ratio of $\tilde{g}\tilde{g}$ production is small, although $\sigma(\tilde{g}\tilde{g})$ may be larger than $\sigma(\tilde{q}\tilde{q})$ in mSUGRA model.

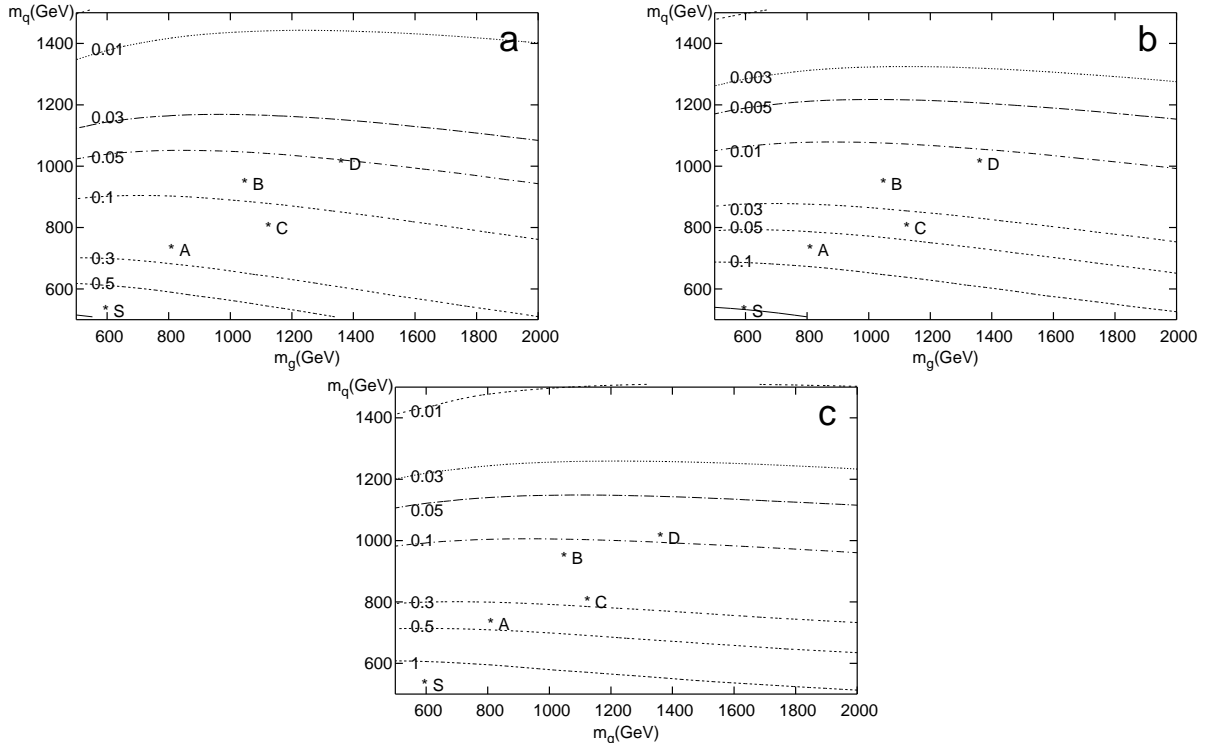


FIG. 4: Contour plot of a) $\sigma(\tilde{q}_L^+\tilde{q}_L^+)$, b) $\sigma(\tilde{q}_L^-\tilde{q}_L^-)$ and c) $\sigma(\tilde{q}_L^+\tilde{q}_L^-)$ as the function of $m_{\tilde{g}}$ and $m_{\tilde{q}}$.

The ratio of $\sigma(\tilde{q}_L^\pm\tilde{q}_L^\pm)/\sigma(\tilde{g}\tilde{q}_L^\pm)$ increases as the gluino gets heavier or the squark gets lighter (Figure 6). When $m_{\tilde{g}} \sim m_{\tilde{q}}$ the ratio is always less than 1/2 for $m_{\tilde{q}} < 1500$ GeV.

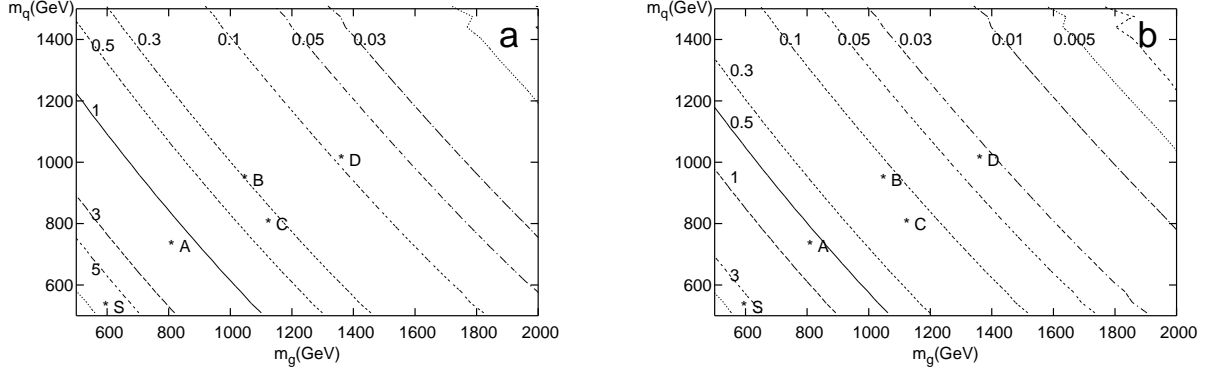


FIG. 5: Contour plot of a) $\sigma(\tilde{g}\tilde{q}_L^+)$ and b) $\sigma(\tilde{g}\tilde{q}_L^-)$ as the function of $m_{\tilde{g}}$ and $m_{\tilde{q}}$.

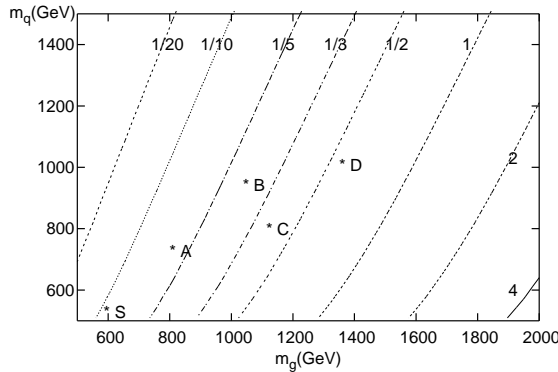


FIG. 6: Contour plot of the $\sigma(\tilde{q}_L^+\tilde{q}_L^+)/\sigma(\tilde{g}\tilde{q}_L^+)$ as the function of $m_{\tilde{g}}$ and $m_{\tilde{q}}$

B. The MSSM model points

The numbers of SS2 l events from $\tilde{g}\tilde{q}_L^\pm$ production and from $\tilde{q}_L^\pm\tilde{q}_L^\pm$ production depend on their decay patterns and the branching ratios. For the study in the following sections, we choose a few model points to fix the branching ratios. We consider the model points with $m_{\tilde{g}} > m_{\tilde{q}}$. If $m_{\tilde{q}} > m_{\tilde{g}}$, both of \tilde{q}_L^\pm decay into \tilde{g} and this \tilde{g} can produce a lepton or an anti-lepton with the same probability, and we cannot distinguish $\tilde{q}^\pm\tilde{q}^\pm$ and $\tilde{q}^+\tilde{q}^-$.

We take relatively heavy sparticle masses ($m_{\tilde{q}}, m_{\tilde{g}} \gtrsim 800$ GeV), because $\sigma(\tilde{q}_L^\pm\tilde{q}_L^\pm)$ is too small compared with $\sigma(\tilde{g}\tilde{q}_L^\pm)$ if the masses are lighter. For example, at SPS1a ($m_{\tilde{q}}, m_{\tilde{g}} \sim 600$ GeV), which is a popular benchmark point defined in [15], $\sigma(\tilde{g}\tilde{q})$ is about ten times as large as $\sigma(\tilde{q}\tilde{q})$. We choose four points A~D shown in Table I so that $\sigma(\tilde{q}_L^+\tilde{q}_L^+)/\sigma(\tilde{g}\tilde{q}_L^+) \lesssim 1/5$, because we find that one can reduce $\tilde{g}\tilde{q}$ background by factor of 1/10 by applying various cuts in Section 3. The points A~D and SPS1a are also marked in Figure 1~6. We can see in Figure 6 that the ratio $\sigma(\tilde{q}_L^+\tilde{q}_L^+)/\sigma(\tilde{g}\tilde{q}_L^+)$ is about 1/6, 1/4, 1/3, 1/2, and 1/10 for Point A~D and SPS1a respectively.

Point A and B are mSUGRA points where $(m_0, m_{\frac{1}{2}})$ are $(100 \text{ GeV}, 340 \text{ GeV})$ and $(100 \text{ GeV}, 450 \text{ GeV})$, $A_0 = 0$, $\tan \beta = 10$, $\text{sign } \mu > 0$ respectively. At these points, the mass difference of $\tilde{\tau}_1$ and $\tilde{\chi}_1^0$ is small. This feature is favored to reduce the LSP abundance. Point C and D are the mSUGRA points where $(m_0, m_{\frac{1}{2}})$ are $(370 \text{ GeV}, 340 \text{ GeV})$ and $(400 \text{ GeV}, 450 \text{ GeV})$, $A_0 = 0$, $\tan \beta = 10$, $\text{sign } \mu > 0$ respectively, except the low energy gluino masses are heavier than the mSUGRA predictions by 300 GeV. By increasing gluino mass, the production cross section of gluino decreases, therefore $\tilde{g}\tilde{q}$ backgrounds are fewer. Sleptons are heavier than the lighter charginos $\tilde{\chi}_1^\pm$, thus the $\tilde{\chi}_1^\pm$ does not decay into a slepton but decays into a W^\pm boson. These points are not favored cosmologically, however the mass density can be reduced by tuning the mass of the pseudoscalar higgs boson m_P as $m_P \sim 2m_{LSP}$ without changing the rate of $SS2l$ signal if we go beyond mSUGRA. Moreover, the decay patterns have some similarity to those predicted in the LHT as we will see later. SPS1a is also written in Table I and II for a reference.

The masses of some particles at our model points are shown in Table I. These spectra are calculated using ISAJET [16, 17]. The other mass spectra are given in the Appendix A 1. The SUSY production cross sections of our model points are also shown in Table II. This is calculated with HERWIG 6.5 [18], where we use CTEQ 6l for PDF [13].

	m_0	$m_{\frac{1}{2}}$	A_0	$m_{\tilde{g}}$	$m_{\tilde{u}_L}$	$m_{\tilde{u}_R}$	$m_{\tilde{t}_1}$	$m_{\tilde{b}_1}$	$m_{\tilde{\tau}}$	$m_{\tilde{l}_L}$	$m_{\tilde{\chi}_1^0}$
Point A	100	340	0	809.86	737.25	714.56	559.18	683.97	160.79	256.36	132.74
Point B	100	450	0	1047.83	951.16	919.51	734.57	883.16	194.28	324.47	179.11
Point C	370	340	0	1123.23	808.67	787.79	585.39	731.10	387.18	437.13	133.95
Point D	400	450	0	1360.22	1017.91	988.10	804.20	928.37	429.40	503.38	180.54
SPS1a	100	250	-100	595.19	537.04	520.45	379.14	491.92	133.39	202.12	96.05

TABLE I: The mass spectra at Point A~D and SPS1a. Here the unit of masses is GeV.

C. The model with an extended gluino sector

In this section, we consider a model with an extended gluino sector. This model was originally considered in [7, 8, 9, 10] as a model with enhanced particle contents of $N = 2$ SUSY to solve the little hierarchy problem. The model has new fermions \tilde{a}_i^a in adjoint

	$\sigma(SUSY)$	$\sigma(\tilde{q}_L^+ \tilde{q}_L^+)$	$\sigma(\tilde{q}_L^- \tilde{q}_L^-)$	$\sigma(\tilde{q}_L^+ \tilde{q}_L^-)$	$\sigma(\tilde{g} \tilde{q}_L^+)$	$\sigma(\tilde{g} \tilde{q}_L^-)$	$\sigma(\tilde{g} \tilde{g})$
Point A	8.621	0.2251	0.0674	0.4247	1.3580	0.6005	0.7134
Point B	2.023	0.0750	0.0189	0.1309	0.2949	0.1208	0.1385
Point C	3.418	0.1321	0.0371	0.2572	0.3410	0.1406	0.0989
Point D	0.963	0.0494	0.0118	0.0875	0.0897	0.0345	0.0280
SPS1a	45.890	0.8033	0.2868	1.600	7.408	3.544	4.872

TABLE II: The SUSY production cross sections for some processes at Point A~D and SPS1a. Here the unit of the cross sections is pb.

representation of each SM gauge groups G_i . The majorana gaugino λ_i^a has a Dirac mass term with \tilde{a}_i^a .

Inspired by the model, we consider phenomenologies of the gluino sector. The mass term of gluino is extended as follows,

$$-\mathcal{L}_{\tilde{g}}^{\text{mass}} = \frac{1}{2} m_{\tilde{g}} \tilde{g} \tilde{g} \rightarrow \frac{1}{2} \begin{pmatrix} \tilde{g} & \tilde{a} \end{pmatrix} \begin{pmatrix} m_g & m_D \\ m_D & m_A \end{pmatrix} \begin{pmatrix} \tilde{g} \\ \tilde{a} \end{pmatrix}. \quad (2)$$

Here, \tilde{g} and \tilde{a} are four component spinors that satisfy the majorana condition. The m_g is a majorana mass for \tilde{g} ,³ m_D is a Dirac mass between \tilde{g} and \tilde{a} , m_A is a majorana mass for \tilde{a} . We leave SU(2) and U(1) gaugino sectors unchanged.

The mass eigenstates \tilde{g}_1, \tilde{g}_2 are majorana particles, and the mass eigenvalues are given as

$$m_{\tilde{g}_{1,2}} = \frac{1}{2} \left(m_g + m_A \pm \sqrt{(m_g - m_A)^2 + 4m_D^2} \right), \quad |m_{\tilde{g}_1}| < |m_{\tilde{g}_2}|. \quad (3)$$

The mass eigenstates are defined as follows,

$$\begin{pmatrix} \tilde{g}_1 \\ \tilde{g}_2 \end{pmatrix} = \begin{pmatrix} \cos \phi & \sin \phi \\ -\sin \phi & \cos \phi \end{pmatrix} \begin{pmatrix} \tilde{g} \\ \tilde{a} \end{pmatrix}, \quad (\tan \phi = \frac{m_{\tilde{g}_1} - m_g}{m_D}). \quad (4)$$

In the limit of $m_D \rightarrow 0, m_A \rightarrow \infty$, \tilde{a} decouples from the MSSM fields, then the phenomenology becomes identical to that of the MSSM. In the limit of $m_g = 0, m_A = 0, m_D \neq 0$ (we call this limit for the pure Dirac limit), the masses of the two gluinos become the same, then \tilde{g}_1 and \tilde{g}_2 interfere strongly so that \tilde{g} and \tilde{a} form a Dirac particle \tilde{g}_D and the anti particle

³ In Ref.[8], $m_{\tilde{g}}$ is taken as zero.

\tilde{g}_D . The model has continuous R-symmetry in the pure Dirac limit. We can assign R-charge 1 for \tilde{g}_D and \tilde{u}_L , -1 for \tilde{u}_R and so on. The pair production of $\tilde{u}_L\tilde{u}_L$, $\tilde{u}_R\tilde{u}_R$ through gluino exchange, which is one of main production process in the MSSM at the LHC, is forbidden by R-charge conservation law. This can be also understood by the fact that existence of nonzero majorana mass of gluino is necessary for $\tilde{q}_L\tilde{q}_L$, $\tilde{q}_R\tilde{q}_R$ processes. While $\tilde{g}_D\tilde{u}_L$ pair production is allowed, $\tilde{g}_D\tilde{u}_L$ pair production is forbidden in the limit, and once \tilde{g}_D is produced, \tilde{g}_D can decay into $\tilde{u}_L\bar{u}$ and $\tilde{d}_L\bar{d}$ but can not decay into \tilde{u}_L^*u nor \tilde{d}_L^*d . The difference between the pure Dirac limit and the MSSM is clear. If m_A , $m_g \ll m_D$, the mass difference of two gluinos $\Delta m_{\tilde{g}_{1,2}}$ is small, continuous R-symmetry exists approximately, and the phenomenology is similar to those in the pure Dirac limit. We do not investigate phenomenology in this case any more.

This model has two gluino like particles. We may be able to observe two gluinos if the mass difference is large enough compared with the decay widths of the gluinos ($\Gamma_{\tilde{g}_{1,2}} \ll \Delta m_{\tilde{g}_{1,2}}$). In this case, each gluino decay produces \tilde{q}^+ and \tilde{q}^- with the same branching ratio. If \tilde{g}_2 is too heavy so that the production cross section is too small to be observed at LHC, we can observe only \tilde{g}_1 . It is not possible in the case to distinguish this model from the MSSM only by the mass spectrum. We focus on this case and study the deviation of the production cross sections from the MSSM predictions. The gluino sector of this model has two degrees of freedom except $m_{\tilde{g}_1}$ and we take them as the other gluino like particle's mass $m_{\tilde{g}_2}$ and the majorana mass m_g .

In Figure 7, we show the production cross sections of SUSY processes such as $\tilde{q}_L^\pm\tilde{q}_L^\pm$ and $\tilde{g}\tilde{q}_L^\pm$ as the functions of majorana gluino mass m_g . Here, we fix $m_{\tilde{g}_2} = -3000$ GeV. and $m_{\tilde{g}_1} = 1047.83$ GeV, which is the gluino mass at Point B. The \tilde{g}_2 cannot be searched for at LHC. We take the mass spectrum of the other sparticles is the same as that of Point B.

In the limit of $m_g = m_{\tilde{g}_1} = 1047.83$ GeV, m_D is zero and $m_{\tilde{g}_2} = m_A = -3000$ GeV. The \tilde{g}_2 decouples from \tilde{q} , and the cross sections involving \tilde{g}_1 are the same as those of Point B. Changing m_g from the value distorts the model from the MSSM. As the majorana mass m_g decreases keeping $m_{\tilde{g}_1}$ and $m_{\tilde{g}_2}$ fixed, the total SUSY production cross section decreases. In particular, $\sigma(\tilde{q}_L^\pm\tilde{q}_L^\pm)$ decreases quickly, while $\sigma(\tilde{g}_1\tilde{q}^\pm)$ decreases linearly because $\sigma(\tilde{g}_1\tilde{q}^\pm)$ is proportional to $\cos^2\phi$ and $m_g = \cos^2\phi(m_{\tilde{g}_1} - m_{\tilde{g}_2}) + m_{\tilde{g}_2}$. The fraction of \tilde{g} in \tilde{g}_2 increases, but \tilde{g}_2 is too heavy so that $\sigma(\tilde{g}_2\tilde{q})$ is small. The $\sigma(\tilde{g}_1\tilde{g}_1)$ is less sensitive to majorana mass m_g . This means that the squark exchange diagram does not contribute much to the cross

section.

When the majorana mass $m_g = 0$, $\sigma(\tilde{q}_L^\pm \tilde{q}_L^\pm)$ is still nonzero value. This is because the majorana mass of the adjoint fermion m_A causes the chirality flip. There are also minor contributions from $\sigma(\tilde{u}_L \tilde{d}_L^*)$ and so on, which are not suppressed by m_g factor.

As m_g decreases further (absolute value $|m_g|$ increases), $\sigma(\tilde{q}_L^\pm \tilde{q}_L^\pm)$ approaches zero around $m_g \sim -1500$ GeV, while $\sigma(\tilde{g}_1 \tilde{q}_L^\pm)$ is reduced by factor of 3. This behavior can be explained by the dependence of the subprocess cross section $\sigma(qq \rightarrow \tilde{q}_L \tilde{q}_L)$ on the mass parameters as follows,

$$\begin{aligned} \sigma(qq \rightarrow \tilde{q}_L \tilde{q}_L) &= \frac{\beta_f}{64\pi s} \int_{-1}^1 d(\cos \theta) \frac{4E^2 g_s^4}{9} \\ &\times |T_{ij}^a T_{kl}^a \{f(m_{\tilde{g}_1}, m_{\tilde{q}}, \mathbf{p}) \cos^2 \phi + f(m_{\tilde{g}_2}, m_{\tilde{q}}, \mathbf{p}) \sin^2 \phi\} \\ &\quad + T_{il}^a T_{kj}^a \{f(m_{\tilde{g}_1}, m_{\tilde{q}}, -\mathbf{p}) \cos^2 \phi + f(m_{\tilde{g}_2}, m_{\tilde{q}}, -\mathbf{p}) \sin^2 \phi\}|^2 \\ &\approx \left| \frac{m_{\tilde{g}_1} \cos^2 \phi}{m_{\tilde{g}_1}^2 + m_{\tilde{q}}^2} + \frac{m_{\tilde{g}_2} \sin^2 \phi}{m_{\tilde{g}_2}^2 + m_{\tilde{q}}^2} \right|^2, \end{aligned} \quad (5)$$

$$\text{where, } f(m_i, m_f, \mathbf{p}) \equiv \frac{m_i}{m_i^2 + m_f^2 + 2|\mathbf{p}|^2 - 2E|\mathbf{p}|\cos\theta} \simeq \frac{m_i}{m_i^2 + m_f^2}. \quad (6)$$

Here $\sigma(qq \rightarrow \tilde{q}_L \tilde{q}_L)$ is the cross section of the subprocess $qq \rightarrow \tilde{q}_L \tilde{q}_L$ with center of mass energy s . The \mathbf{p} is the momentum of one of the created \tilde{q}_L . We set a z-axis along the momentum of one of the initial quarks, θ is a polar angle of \mathbf{p} from the z-axis, and β_f is the beta factor ($\beta_f = \sqrt{1 - 4m_{\tilde{q}}^2/s}$). The T^a denotes a generator of SU(3) group and g_s denotes the gauge coupling. The ϕ is the mixing angle between \tilde{g} and \tilde{a} as defined in (4). In the last line in eq.(5) and the last equality in eq.(6), we take the limit that $|\mathbf{p}| \ll m_{\tilde{q}}$ because $\sigma(pp \rightarrow \tilde{q}_L \tilde{q}_L)$ is dominated by the threshold production. We can calculate that $\sigma(\tilde{q}_L \tilde{q}_L)$ approaches zero around $\phi = \phi_0$ defined as

$$\tan \phi_0 = \sqrt{-\frac{m_{\tilde{g}_1} m_{\tilde{g}_2}^2 + m_{\tilde{q}}^2}{m_{\tilde{g}_2} m_{\tilde{g}_1}^2 + m_{\tilde{q}}^2}}. \quad (7)$$

It is corresponding to $m_g = -1516$ GeV for Point B (here, we use the relation $m_g = \cos^2 \phi m_{\tilde{g}_1} + \sin^2 \phi m_{\tilde{g}_2}$). Note that we again neglect the contributions from chargino and neutralino exchange diagrams in the calculation. They are at most of the order of 10^{-3} pb, and negligible.

The $\sigma(\tilde{q}_L^\pm \tilde{q}_L^\pm)/\sigma(\tilde{g} \tilde{q}_L^\pm)$ is less than 5% in the range of $-1800 \text{ GeV} < m_g < -800 \text{ GeV}$, while $\sigma(\tilde{q}_L^\pm \tilde{q}_L^\pm)/\sigma(\tilde{q}_L^\pm \tilde{q}_L^\pm)$ is about 25% in the MSSM limit ($m_g = 1047.83$ GeV). The production cross

section $\sigma(\tilde{q}_L \tilde{q}_L)$ is reduced by more than factor of 5 compared with $\tilde{g} \tilde{q}_L$ in this range (Figure 8).

As m_g decreases further, $\sigma(\tilde{q}_L^\pm \tilde{q}_L^\pm)$ increases again while $\sigma(\tilde{g}_1 \tilde{q}_L^\pm)$ keeps decreasing. When $m_g = -3000$ GeV, \tilde{g}_2 is \tilde{g} and \tilde{g}_1 is \tilde{a} . In this limit, $\sigma(\tilde{q}_L \tilde{q}_L)$ is enhanced by the factor of m_g in the amplitude, and $\sigma(\tilde{g}_1 \tilde{q}_L^\pm) = 0$ because \tilde{g}_1 does not couple \tilde{q} . We do not discuss this region because the production and decay pattern would be significantly different from the MSSM.

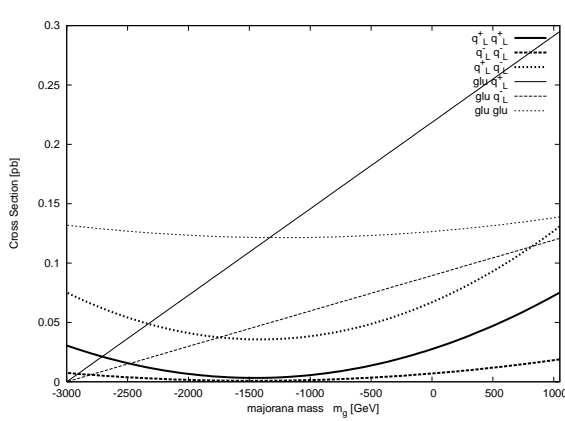


FIG. 7: The production cross sections as the function of the gluino majorana mass m_g for the model with an extended gluino sector. The mass spectrum is the same as that at Point B.

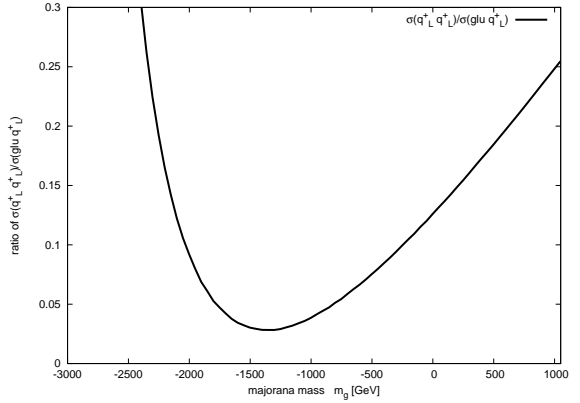


FIG. 8: The ratio of $\sigma(\tilde{q}_L^\pm \tilde{q}_L^\pm)$ and $\sigma(\tilde{g} \tilde{q}_L^\pm)$ as the function of the gluino majorana mass m_g for the model with an extended gluino sector. The mass spectrum is the same as that at Point B.

Note that the mass spectrum is the same as that at Point B for entire m_g in Figure 7. We can detect the deviation from the MSSM only through the measurements of production cross sections such as $\sigma(\tilde{q}_L^\pm \tilde{q}_L^\pm)$, $\sigma(\tilde{g} \tilde{q}_L^\pm)$ or their ratios.

D. The Littlest Higgs model with T-parity

The Littlest Higgs model with T-parity (LHT) [5] is an alternative scenario that solves the quadratic divergence problem for Higgs mass and predicts a stable DM candidate. This model is the extension of the Littlest Higgs model [19]. The features of the Littlest Higgs model are,

1. Higgs bosons are introduced as pseudo Nambu-Goldstone bosons of global symmetry

breaking $SU(5)/SO(5)$. The global symmetry is partially gauged, and the gauge symmetry is $[SU(2) \times U(1)]^2$.

2. The gauge groups are spontaneously broken at scale f as $[SU(2) \times U(1)]^2 \rightarrow SU(2)_L \times U(1)_Y$. Heavy gauge bosons of the broken gauge groups are called as W_H^\pm , Z_H , A_H . The masses are,

$$M_{Z_H} \sim M_{W_H} \simeq gf \left[1 - \frac{v^2}{8f^2} \right], \quad M_{A_H} \simeq \frac{g'f}{\sqrt{5}} \left[1 - \frac{5v^2}{8f^2} \right]. \quad (8)$$

Here, v is the electroweak symmetry breaking scale, $v \simeq 246$ GeV.

3. To cancel the quadratic divergence of Higgs mass, the third generation fermion sector has to be extended to respect the global symmetry of the theory. Especially T_+ has to be introduced as a partner of t quark. The T_+ is a $SU(2)_L$ singlet Dirac fermion.

However, this model suffers from large tree level corrections to the electroweak parameters. Even if the parameters of the models are tuned to reduce the corrections, f becomes large enough so that the fine tuning problem is reintroduced [20, 21]. To solve this problem, the LHT model imposes invariance under the T-parity that corresponds to switching two $[SU(2) \times U(1)]$ gauge groups. Matter sectors are extended so that there is a T-odd partner for each SM fermion.

The T-parity plays the similar role as the R-parity of SUSY model. The Lightest T-parity odd particle (LTP) cannot decay because T-parity is multiplicatively conserved for all vertices. The LTP can be a candidate for DM. Moreover, T-odd particles can be produced only in pair in a collider experiment and each of them must decay into the final states including odd number of T-odd particles. As a result, the final states include at least two LTPs. The collider signal at LHC is the large transverse missing energy \cancel{E}_T just like SUSY.

This model predicts a set of new particles. Among them, the heavy gauge bosons W_H^\pm , Z_H , A_H , the SM fermion partners u_- , d_- , s_- , c_- , b_- , t_- , and the top partner T_- are T-odd. In the following, q_-^+ denotes $\{u_-, c_-, t_-, \bar{d}_-, \bar{s}_-, \bar{b}_-\}$, q_-^- denotes $\{d_-, s_-, b_-, \bar{u}_-, \bar{c}_-, \bar{t}_-\}$, q_- denotes q_-^+ and q_-^- .

No T-odd partner for the $SU(3)$ gauge boson is introduced. On the other hand, the decay pattern of T-odd q_- is similar to that of \tilde{q} in SUSY. According to Ref.[11], about 60% of q_-^+ decays into W_H^+ , 100% of W_H^+ decays into W^+ and 25% of W^+ decays into leptons. Therefore about 15% of q_-^+ decays leptonically. This decay pattern is similar to

that of \tilde{q}_L at Point C. Thus, for the LHT model, we obtain SUSY-like signal as if there are only $\tilde{q}\tilde{q}$ and $\tilde{q}\tilde{q}^*$ productions at LHC. Although there is no t-channel colored particle exchange, $\sigma(q_-q_-)$ is non zero due to the t-channel exchange of W_H and A_H . It is higher than that of the MSSM because q_- 's are fermions. For example, $\sigma(q_-^+q_-^+)$ is 0.7 pb, $\sigma(q_-^-q_-^-)$ is 0.15 pb at $M_{q_-} = 800$ GeV and $f = 560$ GeV, and $\sigma(q_-^+q_-^-)$ is 0.2 pb, $\sigma(q_-^-q_-^-)$ is 0.04 pb at $M_{q_-} = 1000$ GeV and $f = 700$ GeV. The $\sigma(q_-^+q_-^+)$ is $4 \sim 5$ times as large as $\sigma(\tilde{q}^+\tilde{q}^+)$ at the MSSM model points with the same mass scale (See Figure 4a). The ratio $\sigma(q_-^+q_-^+)/\sigma(q_-^-q_-^-)$ is similar to $\sigma(\tilde{q}^+\tilde{q}^+)/\sigma(\tilde{q}^-\tilde{q}^-)$ of the MSSM. The ratio $\sigma(l^+l^+)/\sigma(l^-l^-)$ of the LHT is expected to be higher than that of the MSSM, because $\tilde{g}\tilde{q}$ production dominates the total SUSY productions. As we will see later, production cross sections and their ratios will help to distinguish the LHT and the MSSM.

E. Summary of the production cross sections

There are several models which predict the MSSM-like collider signature with large \cancel{E}_T .

In section 2.2 we have shown that $\tilde{q}_L\tilde{q}_L$ production cross section changes significantly if majorana mass contribution to the gluino mass is reduced in the model with an extended gluino sector. In particular in case of $m_g < m_{\tilde{g}_1}$, $\sigma(\tilde{q}_L\tilde{q}_L)$ can be reduced significantly compared with $\sigma(\tilde{g}\tilde{q}_L)$.

On the other hand, for the LHT model, q_- may have similar decay pattern to \tilde{q} while there is no particle corresponding to gluino. Hence, the signal is similar to that of the MSSM with undetectably heavy gluino. The $\sigma(q_-q_-)$ is larger than the $\sigma(\tilde{q}\tilde{q})$ by factor of 5.

The signal cross sections of these models are different from that of the MSSM, even if the mass spectrum is the same. Therefore the $\sigma(\tilde{q}_L\tilde{q}_L \rightarrow l^\pm l^\pm X)$ is one of the key observables for the MSSM studies.

III. SEPARATION OF $\tilde{q}\tilde{q}$ AND $\tilde{g}\tilde{q}$ PRODUCTIONS

A. Branching ratios of \tilde{q} , \tilde{g}

To identify the $\tilde{q}_L\tilde{q}_L$ production (mainly $\tilde{u}_L\tilde{u}_L$ production), $\tilde{q}_L\tilde{q}_L \rightarrow 2lX$ events would be useful because $\mathcal{BR}(\tilde{q}_L^\pm \rightarrow l^\pm X) \gg \mathcal{BR}(\tilde{q}_L^\pm \rightarrow l^\mp X)$. The signal rate depends on the leptonic

branching ratios of sparticles. The branching ratios at Point A~D are shown in Appendix A 2. We summarize them in Table III.

mode	BR(%)			
	Point A	Point B	Point C	Point D
$\tilde{g} \rightarrow \tilde{q}_L^+ q$	11	10	14	13
$\rightarrow \tilde{q}_L^- q$	11	10	14	13
$\rightarrow \tilde{q}_R q$	38	36	32	32
$\rightarrow \tilde{q}_3 q_3$	41	45	40	41
$\tilde{u}_L \rightarrow l^+ X$	31	46	18	17
$\tilde{d}_L \rightarrow l^- X$	30	44	17	17
$\tilde{b}_1 \rightarrow l^- X$	28	39	17	20
$\tilde{b}_2 \rightarrow l^- X$	22	27	11	12
$\tilde{t}_1 \rightarrow l^+ X$	29	37	17	10
$\tilde{t}_2 \rightarrow l^+ X$	18	23	6.3	11

TABLE III: Branching ratios of squarks and gluinos at Point A~D. These are calculated by ISAJET. Here, \tilde{q}_L^+ denotes $\{\tilde{u}_L, \tilde{d}_L^*, \tilde{c}_L, \tilde{s}_L^*\}$, \tilde{q}_L^- denotes the antiparticles of \tilde{q}_L^+ , \tilde{q}_R denotes $\{\tilde{u}_R, \tilde{d}_R, \tilde{c}_R, \tilde{s}_R\}$ and their antiparticles. \tilde{q}_3 denotes $\{\tilde{b}_1, \tilde{b}_2, \tilde{t}_1, \tilde{t}_2\}$ and the antiparticles of them. X means LSP and other SM particles.

We can see that \tilde{q}_L^\pm produces l^\pm when \tilde{q}_L^\pm decays through chargino. The $\mathcal{BR}(\tilde{q}_L^\pm \rightarrow l^\pm)$ is about 30% at Point A. If \tilde{q}_L^\pm decays through neutralino, \tilde{q}_L^\pm may also produce l^\mp .

On the other hand, a gluino decays into third generation squarks \tilde{q}_3 more than the 1st, 2nd generation squarks \tilde{q}_L , and also decays into \tilde{q}_R more than \tilde{q}_L at these points, because gluino and squark masses are close and the phase space of the gluino decay is sensitive to the small difference of squark masses. (The third generation squarks \tilde{t}, \tilde{b} are lighter than the 1st, 2nd generation \tilde{q}_L , and \tilde{q}_R is lighter than \tilde{q}_L .) We also find $\mathcal{BR}(\tilde{g} \rightarrow l^+) = \mathcal{BR}(\tilde{g} \rightarrow l^-)$ and they are small (8%), because \tilde{g} decays dominantly into \tilde{q}_R . As a result, $\mathcal{BR}(\tilde{q}_L^+ \tilde{q}_L^+ \rightarrow l^+ l^+)$ is 9%, $\mathcal{BR}(\tilde{g} \tilde{q}_L^+ \rightarrow l^+ l^+)$ is 2.4%, $\mathcal{BR}(\tilde{g} \tilde{g} \rightarrow l^+ l^+)$ is 0.6% at Point A.

To measure $\sigma(\tilde{q}_L^+ \tilde{q}_L^+)$, we need to reduce the events involving \tilde{g} by appropriate cuts. We can achieve it in part by rejecting events with b -tagged jets because $\mathcal{BR}(\tilde{g} \rightarrow \tilde{t} \text{ or } \tilde{b})$ is large; $\mathcal{BR}(\tilde{g} \rightarrow l \text{ without } b\text{-quark})$ is only 6%. For pair production processes, $\mathcal{BR}(\tilde{q}_L^+ \tilde{q}_L^+ \rightarrow l^+ l^+ \text{ without } b\text{-quark})$ is $\sim 9\%$, $\mathcal{BR}(\tilde{g} \tilde{q}_L^+ \rightarrow l^+ l^+ \text{ without } b\text{-quark}) \sim 1\%$, $\mathcal{BR}(\tilde{g} \tilde{g} \rightarrow l^+ l^+ \text{ without } b\text{-quark}) \sim 0.1\%$. However, the efficiency of b -veto is at most 60%.

In the following, we neglect SS2l events from $\tilde{g} \tilde{g}$ production. It is reasonable if squark and gluino masses are sufficiently large, such as at Point A \sim D, because the $\sigma(\tilde{g} \tilde{g})$ is small

(Table II) and $\mathcal{BR}(\tilde{g} \rightarrow \tilde{q}_L) \ll 1$. Furthermore, the events contain more b -jets in average.

B. Events generation and detector simulation

We generate about 300,000 SUSY events by HERWIG 6.5 [18] at Point A~D and SPS1a. Number of events actually produced by HERWIG and the corresponding integrated luminosities are listed in Table IV. The $N(\tilde{q}_L^+ \tilde{q}_L^+) : N(\tilde{q}_L^- \tilde{q}_L^-)$ is about 4:1 and the $N(\tilde{g} \tilde{q}_L^+) : N(\tilde{g} \tilde{q}_L^-)$ is about 2:1 for these model points as discussed in Sec II A.

	$N(SUSY)$	$N(\tilde{q}_L^+ \tilde{q}_L^+)$	$N(\tilde{q}_L^+ \tilde{q}_L^-)$	$N(\tilde{q}_L^- \tilde{q}_L^-)$	$N(\tilde{g} \tilde{q}_L^+)$	$N(\tilde{g} \tilde{q}_L^-)$	$N(\tilde{g} \tilde{g})$	$\int dt \mathcal{L}$
Point A	289906	7865	10698	2197	44007	19330	21065	33.63
Point B	284544	10601	11115	2526	39208	15818	13242	140.65
Point C	295042	11411	14666	3072	25793	10729	4748	86.32
Point D	295695	14505	14394	3279	23589	8982	3333	307.06
SPS1a	293161	5412	10423	1849	46072	22241	31371	6.39

TABLE IV: Numbers of the events generated by HERWIG 6.5

We use AcerDET [22] for event reconstruction. AcerDET is a fast simulation and reconstruction package. It finds jets, isolated electrons, muons, photons and calculate missing transverse energy from particles in the events. The granularity of the calorimetric cells is assumed as (0.1×0.1) in $(\eta \times \phi)$ coordinates for $|\eta| < 3.2$. The clusters with $p_T > 15 \text{ GeV}$ for $\Delta R_{\text{cone}} = 0.4$ are classified as jets. It also labels a jet as a b -jet if a b -quark of a momenta $p_T > 5 \text{ GeV}$ is found within the cone $\Delta R = 0.2$. The tagging efficiency of the algorism is about 80% and it is too high compared with full simulation result 60% in ATLAS. Therefore we assume that 60% of the b -labeled jet is tagged. Isolation criteria for muons, electrons and photons are $p_T > 10 \text{ GeV}$ and $|\eta| < 2.5$, separation by $\Delta R > 0.4$ from other clusters and $\sum E_T < 10 \text{ GeV}$ in a cone $\Delta R < 0.2$ around them. For electrons and photons, we require $\Delta R_{\text{cluster}} < 0.1$.

The \cancel{E}_T is calculated by summing the transverse momenta of all clusters and cells not used for clusters reconstruction as follows,

$$\cancel{E}_T = \left| \sum_{\text{visible}} \mathbf{p}_T \right|. \quad (9)$$

The numbers of the SS2 l events from each production process are shown in Table V for Point B.

Point B	generated	l^+l^+			l^-l^-		
		all	c_0	c_1	all	c_0	c_1
total	284544	4363	2573	1680	2231	1288	749
$\tilde{q}_L^+\tilde{q}_L^+$	10601	1410	967	958	6	2	2
$\tilde{q}_L^-\tilde{q}_L^-$	2526	1	1	1	399	264	258
$\tilde{q}_L^+\tilde{q}_L^-$	11115	88	54	52	112	70	68
$\tilde{g}\tilde{q}_L^+$	39208	1720	1067	467	149	84	31
$\tilde{g}\tilde{q}_L^-$	15818	46	31	14	732	469	235
$\tilde{g}\tilde{g}$	13242	220	117	22	225	121	26

TABLE V: Numbers of SS2 l events from each production process at Point B

Here, all, c_0 and c_1 denote the different cuts applied to the events,

all : all SS2 l events generated by HERWIG 6.5.

c_0 : basic cuts, $\not{E}_T > 200$ GeV, $M_{\text{eff}} > 500$ GeV, $\not{E}_T > 0.2M_{\text{eff}}$ and $n_{100} \geq 2$

(n_{100} is the number of jets with $p_T \geq 100$ GeV)

c_1 : c_0 and $n_b = 0$. (n_b is the number of b -tagged jets.)

M_{eff} is defined as,

$$M_{\text{eff}} = \sum_{\substack{\text{jets} \\ |\mathbf{p}_T| \geq 50 \text{ GeV}}} |\mathbf{p}_T| + \sum_{\substack{\text{leptons} \\ |\mathbf{p}_T| \geq 10 \text{ GeV}}} |\mathbf{p}_T| + \not{E}_T. \quad (10)$$

The SS2 l events are mainly produced from $\tilde{q}_L^\pm\tilde{q}_L^\pm$, $\tilde{g}\tilde{q}_L^\pm$, $\tilde{g}\tilde{g}$.⁴ We find that $N(l^+l^+$ from $\tilde{q}_L^\pm\tilde{q}_L^\pm$): $N(l^-l^-$ from $\tilde{q}_L^-\tilde{q}_L^-$) is nearly 4:1 and $N(l^+l^+$ from $\tilde{g}\tilde{q}_L^\pm$): $N(l^-l^-$ from $\tilde{g}\tilde{q}_L^-$) is nearly 2:1. Note that $l^\pm l^\pm$ events are also produced from $\tilde{q}^+\tilde{q}^-$, if \tilde{q} decay into a neutralino and the neutralino decays into $\tau^+\tau^-$. After c_0 cut, contributions from $\tilde{q}_L^\pm\tilde{q}_L^\pm$, $\tilde{q}_L^+\tilde{q}_L^-$, $\tilde{g}\tilde{q}_L^\pm$, $\tilde{g}\tilde{g}$ dominate SS2 l events. We describe the number of the generated $l^\pm l^\pm$ events after cut c_i as $N(l^\pm l^\pm; c_i)$. Compared $N(l^\pm l^\pm; c_0)$ with $N(l^\pm l^\pm; c_1)$, we see b -veto cut (c_1) reduces only events involving

⁴ The other SS2 l events come mainly from productions involving the third generation squarks, charginos and gluino.

\tilde{g} . The l^+l^+ events from $\tilde{g}\tilde{q}^\pm$ are reduced by half. The l^+l^+ events from $\tilde{g}\tilde{g}$ are reduced by one fifth. After c_1 cut, l^+l^+ events from $\tilde{q}^+\tilde{q}^+$ are 60% of all l^+l^+ events, while they are 40% under c_0 cut.

C. Hemisphere cuts

To reduce events involving \tilde{g} further, we next study numbers of jets emitted from \tilde{q} and \tilde{g} . A gluino decays into a squark and a quark, and the squark decays into a chargino or a neutralino and a quark. Thus, a gluino usually emits at least two jets while a squark emits at least one jet. We can distinguish the parent particles by the number of high p_T jets in the events. In this paper, we divide final state particles into two groups called hemispheres, then we investigate the number of jets and the invariant masses in each hemisphere.

SUSY production processes always occur in pair by the R-parity conservation. Particles from each sparticle decay with momentum p_i, p_j, \dots are kinematically constrained so that $(p_i + p_j + \dots)^2 = m^2$ where m is the mass of the parent sparticle. When the parent sparticle is boosted the decay products are boosted in the same direction. We therefore divide all high p_T object into two groups: hemisphere 1 $\{p_{1k}\}$, hemisphere 2 $\{p_{2k}\}$, which satisfy the following conditions.

Any $p_{1i} \in \{p_{1k}\}$, $p_{2i} \in \{p_{2k}\}$ satisfy the conditions

$$\begin{aligned} d(p_{1,\text{ax}}, p_{1i}) &\leq d(p_{2,\text{ax}}, p_{1i}), \\ d(p_{2,\text{ax}}, p_{2i}) &\leq d(p_{1,\text{ax}}, p_{2i}). \end{aligned} \quad (11)$$

We define the axis of hemisphere p_{ax} and the distance between two 4-vectors $d(p_1, p_2)$ as follows.

$$p_{1,\text{ax}} \equiv \sum_i p_{1i}, \quad p_{2,\text{ax}} \equiv \sum_i p_{2i}, \quad (12)$$

$$d(p_{\text{ax}}, p_i) \equiv \frac{(E_{\text{ax}} - |\mathbf{p}_{\text{ax}}| \cos \theta_i) E_{\text{ax}}}{(E_{\text{ax}} + E_i)^2} \quad (\text{Here, } \theta_i \text{ is the angle between } \mathbf{p}_{\text{ax}} \text{ and } \mathbf{p}_i). \quad (13)$$

Here, high p_T objects mean jets with $p_T \geq 50 \text{ GeV}$ and $\eta \leq 3$, leptons, photons with $p_T \geq 10 \text{ GeV}$ and $\eta \leq 2.5$.

Our algorithm to find the hemisphere axes is as follows. We take the highest p_T object in the event and regard its momentum as $p_{1,\text{ax}}$. Next, $p_{2,\text{ax}}$ is taken as the momentum of the object which has largest $|\mathbf{p}|\Delta R$, where \mathbf{p} is the momentum of a object, $\Delta R \equiv \sqrt{(\Delta\eta)^2 + (\Delta\phi)^2}$, and $\Delta\eta$ and $\Delta\phi$ are the differences of the pseudo-rapidity and cylindrical angle of the \mathbf{p} from $\mathbf{p}_{1,\text{ax}}$ respectively. We calculate $d(p_{1,\text{ax}}, p)$ and $d(p_{2,\text{ax}}, p)$ for all high p_T objects. We identify it to hemisphere 1 if $d(p_{1,\text{ax}}, p) < d(p_{2,\text{ax}}, p)$. Otherwise, to hemisphere 2. After that, we redefine $p_{1,\text{ax}}$ and $p_{2,\text{ax}}$ as the new hemisphere axes by using eq.(12). We iterate the same operation using new $p_{1,\text{ax}}$ and $p_{2,\text{ax}}$ five times.

After determination of two hemispheres, we calculate the maximum invariant mass m_{jj} of all jet pairs in a hemisphere. We call it m_{jj1} for hemisphere 1 and m_{jj2} for hemisphere 2. When a hemisphere has only one or zero jet, we define $m_{jj} = 0$.

The 2-dim plots of m_{jj1} vs. m_{jj2} for production processes $\tilde{g}\tilde{g}$, $\tilde{g}\tilde{u}_L$, $\tilde{u}_L\tilde{u}_L$ at Point B are shown in Figure 9a~c. Here, the plotted events are not only SS2l events but all events after imposing c_0 cut.

We find $\tilde{g}\tilde{g}$ events are mainly distributed in the region of $m_{jj1} \neq 0$ and $m_{jj2} \neq 0$, $\tilde{g}\tilde{q}$ events are mainly distributed in the region of either $m_{jj1} = 0$ or $m_{jj2} = 0$, $\tilde{q}\tilde{q}$ events are mainly distributed in the region of $m_{jj1} = m_{jj2} = 0$. This is because \tilde{g} produces two high p_T jets while \tilde{q} produces only one high p_T jet. Therefore we require $m_{jj1} = m_{jj2} = 0$ as the cut to reduce \tilde{g} production events.

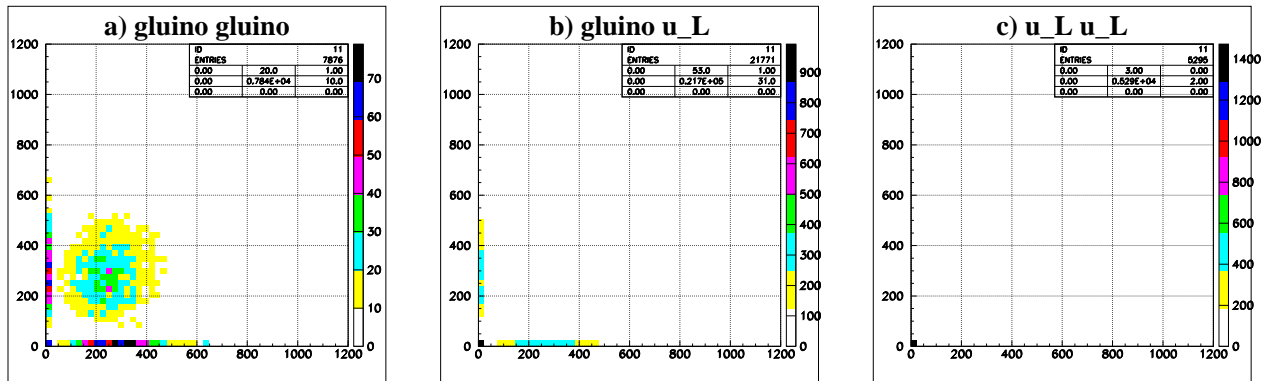


FIG. 9: m_{jj1} vs. m_{jj2} distribution for a) $\tilde{g}\tilde{g}$, b) $\tilde{g}\tilde{u}_L$, c) $\tilde{u}_L\tilde{u}_L$ production events.

D. Numerical results after hemisphere cuts

We apply the cuts $m_{jj1} = 0$ and/or b -veto on the $SS2l$ events and investigate the efficiencies for each production channel. We apply the cuts subsequently to remove the contributions from $\tilde{g}\tilde{q}$ production, while keeping the contributions from $\tilde{q}\tilde{q}$. We define cuts $c_2 \sim c_5$ in addition to c_0 and c_1 as follows,

- c_2 : c_0 with $\min(m_{jj1}, m_{jj2}) = 0$.
- c_3 : c_0 with $m_{jj1} = m_{jj2} = 0$.
- c_4 : $c_0, n_b = 0$ and $\min(m_{jj1}, m_{jj2}) = 0$.
- c_5 : $c_0, n_b = 0$ and $m_{jj1} = m_{jj2} = 0$.
- ratio : $N(c_5)/N(c_0)$. This describes the efficiency for c_5 cut.

The number of the $SS2l$ events after these cuts are shown in the Table VI. The cut requiring $m_{jj1} = 0$ or $m_{jj2} = 0$ (c_2, c_4) reduces $\tilde{g}\tilde{g}$ events drastically and $\tilde{g}\tilde{q}$ events moderately. The cut requiring $m_{jj1} = 0$ and $m_{jj2} = 0$ (c_3, c_5) further reduces $\tilde{g}\tilde{q}$ events. On the other hand, $\tilde{q}\tilde{q}$ events survive under the cut c_5 compared with $\tilde{g}\tilde{g}$, $\tilde{g}\tilde{q}$ events. Note that a b -veto cut is not essential to reduce the gluino contribution. The cut c_3 reduces events involving gluino less than $\tilde{q}_L\tilde{q}_L$ events although b -veto is not applied. The $\tilde{g}\tilde{q}$ events are dominant under c_0 cut and $\tilde{q}\tilde{q}$ events are dominant under c_5 cut.

Point A	all	c_0	c_1	c_2	c_3	c_4	c_5	ratio
l^+l^+ total	1519	716	349	463	114	267	94	0.131
$\tilde{q}\tilde{q}$	235	140	132	123	57	117	56	0.400
$\tilde{g}\tilde{q}$	618	333	125	205	27	83	16	0.048
$\tilde{g}\tilde{g}$	184	79	14	27	2	5	0	0.000
l^-l^- total	1213	610	286	368	89	216	75	0.123
$\tilde{q}\tilde{q}$	151	92	90	83	42	81	41	0.446
$\tilde{g}\tilde{q}$	472	262	108	159	19	75	13	0.050
$\tilde{g}\tilde{g}$	172	93	20	31	1	6	0	0.000

Point B	all	c_0	c_1	c_2	c_3	c_4	c_5	ratio
l^+l^+ total	4363	2573	1612	1765	465	1293	441	0.171
$\tilde{q}\tilde{q}$	1479	1014	1001	894	363	883	361	0.356
$\tilde{g}\tilde{q}$	1765	1098	433	613	52	279	36	0.033
$\tilde{g}\tilde{g}$	220	117	18	26	1	5	0	0.000
l^-l^- total	2231	1288	708	809	187	561	171	0.133
$\tilde{q}\tilde{q}$	499	326	316	286	122	278	121	0.371
$\tilde{g}\tilde{q}$	861	541	237	304	23	169	15	0.028
$\tilde{g}\tilde{g}$	225	121	22	32	0	11	0	0.000

Point C	all	c_0	c_1	c_2	c_3	c_4	c_5	ratio
l^+l^+ total	1081	467	242	284	66	186	62	0.133
$\tilde{q}\tilde{q}$	259	154	144	133	57	127	57	0.370
$\tilde{g}\tilde{q}$	327	165	55	69	3	29	2	0.012
$\tilde{g}\tilde{g}$	47	10	1	2	0	0	0	0.000
l^-l^- total	618	233	110	134	20	83	17	0.073
$\tilde{q}\tilde{q}$	77	40	39	37	12	36	12	0.300
$\tilde{g}\tilde{q}$	164	66	23	29	2	14	0	0.000
$\tilde{g}\tilde{g}$	32	11	3	6	0	2	0	0.000

Point D	all	c_0	c_1	c_2	c_3	c_4	c_5	ratio
l^+l^+ total	1157	571	318	335	82	243	78	0.137
$\tilde{q}\tilde{q}$	356	216	207	182	72	179	72	0.333
$\tilde{g}\tilde{q}$	333	169	56	64	2	26	2	0.012
$\tilde{g}\tilde{g}$	35	18	5	7	0	4	0	0.000
l^-l^- total	588	263	116	128	27	83	24	0.091
$\tilde{q}\tilde{q}$	84	55	47	45	16	40	16	0.291
$\tilde{g}\tilde{q}$	131	63	25	23	1	14	1	0.016
$\tilde{g}\tilde{g}$	27	9	0	0	0	0	0	0.000

sps1a	all	c_0	c_1	c_2	c_3	c_4	c_5	ratio
l^+l^+ total	1314	461	250	326	80	193	63	0.137
$\tilde{q}\tilde{q}$	164	72	71	59	29	58	28	0.389
$\tilde{g}\tilde{q}$	550	226	106	150	22	75	15	0.066
$\tilde{g}\tilde{g}$	155	58	15	32	2	9	2	0.034
l^-l^- total	1070	345	180	242	64	147	46	0.133
$\tilde{q}\tilde{q}$	109	47	45	41	16	40	16	0.340
$\tilde{g}\tilde{q}$	394	156	64	109	27	51	16	0.103
$\tilde{g}\tilde{g}$	147	39	9	17	2	7	0	0.000

TABLE VI: Numbers of SS2 l events after the cuts for Point A~D and SPS1a. Here, c_0 is set as $\cancel{E}_T > 200 \text{ GeV}$, $M_{\text{eff}} > 500 \text{ GeV}$, $\cancel{E}_T > 0.2M_{\text{eff}}$, $n_{100} \geq 2$.

The ratio of $N(l^+l^+; c_5)/N(l^+l^+; c_0)$ for $\tilde{q}\tilde{q}$ productions is more than 30% at our model points. It is $3 \sim 5\%$ for $\tilde{g}\tilde{q}$ production at Point A and B and about 1% at Point C and D. We can obtain a pure SS2l event set from $\tilde{q}\tilde{q}$ production by the c_5 cut. Dominant contributions to $N(l^+l^+ \text{ from } \tilde{q}\tilde{q})$ are from $\tilde{q}_L\tilde{q}_L$ productions (mainly $\tilde{u}_L\tilde{u}_L$). We can see in Appendix A3, $N(l^+l^+ \text{ from } \tilde{u}_L\tilde{u}_L \text{ and } \tilde{u}_L\tilde{c}_L) = 1256$, $N(l^+l^+ \text{ from } \tilde{u}_L\tilde{d}_L^* \text{ and } \tilde{u}_L\tilde{s}_L^*) = 138$, $N(l^+l^+ \text{ from } \tilde{u}_L\tilde{d}_L) = 84$ are obtained among $N(l^+l^+ \text{ from all } \tilde{q}\tilde{q}) = 1479$ at Point B. In Table VI, we also show the results at SPS1a for a reference. The efficiencies of these cuts are similar to the other points. However contamination from $\tilde{g}\tilde{q}$ production is larger.

Experimentally, we can only observe total SS2l events. The ratio $N(l^+l^+; c_5)/N(l^+l^+; c_0)$ for total events is $13\sim17\%$ at our points. If there is no $\tilde{q}_L\tilde{q}_L$ production, it becomes less than 5%. If the efficiency of $N(l^+l^+; c_5)/N(l^+l^+; c_0)$ for $\tilde{q}\tilde{q}$ and $\tilde{g}\tilde{q}$ can be obtained by MC simulations and from the other constraints, we may estimate $\sigma(\tilde{q}_L\tilde{q}_L)$ from $N(l^\pm l^\pm)$. The model parameters we need are gluino, squark masses to constrain the branching ratio of gluino, leptonic branching ratios of squarks and decay kinematics of them. Ratio of the events with 2 leptons to the events with 1 lepton should be useful to estimate the leptonic branching ratio of \tilde{q} . The decay cascade $\tilde{g} \rightarrow \tilde{b}\bar{b}(\tilde{t}\bar{t}) \rightarrow \tilde{\chi}^- t\bar{b}(\tilde{\chi}^+ \bar{t}b)$ also emits leptons from W^\pm decays. The branching ratio must be estimated carefully from b -tagged samples. Estimation on the errors of the branching ratio is beyond the scope of this paper. Information on the mass would be obtained from various end points of the decay distributions [23, 24, 25, 26, 27, 28]. In addition, there are various sources of systematic errors for the cross sections such as the PDF, NNLO corrections and so on. Following the arguments in [6], we assume overall uncertainty on the total production cross section is 17%, which comes from 10% PDF uncertainty, 8% NNLO corrections [29] and 10% $\sigma(\tilde{q}_L\tilde{q}_L)$ error from 3% squark mass uncertainty. If the squark mass error is 10%, $\sigma(\tilde{q}_L\tilde{q}_L)$ error is 40%, then this uncertainty dominates the systematic errors.

Uncertainties on the cross sections may partly cancel in $N(l^\pm l^\pm; c_5)/N(l^\pm l^\pm; c_0)$ ratios. The errors on the absolute sparticle masses are common for both $\sigma(\tilde{q}_L\tilde{q}_L)$ and $\sigma(\tilde{g}\tilde{q}_L)$, and $m_{\tilde{g}} - m_{\tilde{q}}$ may be known precisely. If the cross section errors cancel, the total systematic error becomes 14%. Uncertainties on leptonic branching ratios of squarks may also partly cancel because gluino emits leptons through its decay into a squark.

Note that the ratio of the production cross section of $\tilde{g}\tilde{u}_L$ to $\tilde{g}\tilde{d}_L$ is 2:1, and that of $\tilde{u}_L\tilde{u}_L$ to $\tilde{d}_L\tilde{d}_L$ is 4:1. Indeed, at Point C, D, the ratio $N(l^+l^+; c_5)$ to $N(l^-l^-; c_5)$ is 4:1, while that

is 2:1 for c_0 . At Point A (B), the ratio of $N(l^+l^+; c_5)$ to $N(l^-l^-; c_5)$ is 5:4 (5:2), while the ratio of $N(l^+l^+; c_0)$ to $N(l^-l^-; c_0)$ is 7:6 (2:1). These discrepancies from $\sigma(\tilde{q}^+\tilde{q}^+)/\sigma(\tilde{q}^-\tilde{q}^-)$ or $\sigma(\tilde{g}\tilde{q}^+)/\sigma(\tilde{g}\tilde{q}^-)$ in Table IV are caused by decays of the second lightest neutralinos from \tilde{q}_L^\pm . According to Appendix A 2, the left handed squark can decay into $\tilde{\chi}_1^0\tau^+\tau^-$ through $\tilde{\chi}_2^0$ with large branching ratio at Point A (B). Therefore there is a contamination from $\tilde{q}_L^+\tilde{q}_L^-$ (mainly $\tilde{u}_L\tilde{d}_L$) productions to SS2 l events and the ratio of $N(l^+l^+)$ to $N(l^-l^-)$ gets closer to 1:1. Therefore the charge of the hard lepton does not reflect the sign of the parent particle.

E. Tight cut for heavy mass spectrum

We now consider the SM background to the SS2 l events. Here we only consider $t\bar{t}$ production which is found as dominant background in [6]. The background comes from the events that one lepton comes from leptonic decays of a top quark while the other lepton comes from accidental sources such as b quark decays. The $\mathcal{BR}(t \rightarrow l^-)$ is small, but, total number of $t\bar{t}$ events is significantly larger than the signal ($\sigma(t\bar{t}) = 400$ pb in tree level). The $t\bar{t}$ events corresponding to 100 fb^{-1} are also generated by HERWIG 6.5, and the result is shown in Table VII.

$t\bar{t}$	all	c_0	c_1	c_2	c_3	c_4	c_5	ratio
l^+l^+	1710	152	70	133	32	65	17	0.112
l^-l^-	1635	146	76	133	20	70	10	0.068

TABLE VII: Numbers of the SS2 l events from $t\bar{t}$ production after the cuts $c_0 \sim c_5$ for $\int dt \mathcal{L} = 100\text{ fb}^{-1}$. Here, $c_0 \sim c_5$ are the same as Table 6.

At Point A,B, $N(l^+l^+ \text{ from } t\bar{t}; c_0)$ is less than 8% of $N(l^+l^+ \text{ from SUSY}; c_0)$ and $N(l^+l^+ \text{ from } t\bar{t}; c_5)$ is about 5% of $N(l^+l^+ \text{ from SUSY}; c_5)$. At Point C, it is 30% after c_0 , and 25% after c_5 . At Point D, they are ~ 1 . In that case, more strict \cancel{E}_T and M_{eff} cuts are needed.

In Table VI, we have taken $\cancel{E}_T > 200\text{ GeV}$, $M_{\text{eff}} > 500\text{ GeV}$ and $\cancel{E}_T > 0.2M_{\text{eff}}$ as c_0 cut. Numbers of $t\bar{t}$ after various \cancel{E}_T and M_{eff} cuts are shown in Table VIII. The $t\bar{t}$ background is dramatically reduced if high \cancel{E}_T cuts are applied for large M_{eff} [30]. Here, we change the c_0 cut as follows.

\not{E}_T and M_{eff} cuts

$$\begin{aligned}
c^{(1)} &: \not{E}_T > 200 \text{ GeV}, \not{E}_T > 0.2M_{\text{eff}}, M_{\text{eff}} > 500 \text{ GeV} \\
c^{(2)} &: \not{E}_T > 250 \text{ GeV}, \not{E}_T > 0.2M_{\text{eff}}, M_{\text{eff}} > 750 \text{ GeV} \\
c^{(3)} &: \not{E}_T > 300 \text{ GeV}, \not{E}_T > 0.2M_{\text{eff}}, M_{\text{eff}} > 1000 \text{ GeV}
\end{aligned}$$

Number of high p_T jets

$$n_{100} \geq 2 : \text{at least two jets with } p_T > 100 \text{ GeV}$$

$$n_{200} \geq 2 : \text{at least two jets with } p_T > 200 \text{ GeV}$$

number of jet	all	$n_{100} \geq 2$			$n_{200} \geq 2$		
$\not{E}_T, M_{\text{eff}}$ cut	all	$c^{(1)}$	$c^{(2)}$	$c^{(3)}$	$c^{(1)}$	$c^{(2)}$	$c^{(3)}$
$N(l^+l^+ \text{ from } t\bar{t}; c_0)$	1710	152	38	9	13	6	4
$N(l^+l^+ \text{ from } t\bar{t}; c_5)$	*	17	1	0	3	0	0
$N(l^-l^- \text{ from } t\bar{t}; c_0)$	1635	146	43	15	11	8	2
$N(l^-l^- \text{ from } t\bar{t}; c_5)$	*	10	2	1	0	0	0

TABLE VIII: Numbers of the SS2l events from $t\bar{t}$ events after various c_0 cuts for 100 fb^{-1} .

We also show $N(l^\pm l^\pm; c_5)/N(l^\pm l^\pm; c_0)$ after the cut $c^{(i)}$ and the cuts on the number of high p_T jets at Point D in Table IX. The numbers of events are corresponding to 307.06 pb^{-1} . We can see that the efficiency $N(l^\pm l^\pm; c_5)/N(l^\pm l^\pm; c_0)$ for $\tilde{q}\tilde{q}$ production and the efficiency for $\tilde{g}\tilde{q}$ production only weakly depend on the basic cut $c^{(i)}$ and the cuts on the number of high p_T jets. The c_5 cut is still useful to reduce $\tilde{g}\tilde{q}$ productions.

We can drop $t\bar{t}$ background without reducing the signal from SUSY events so much by taking $c^{(3)}$ and $n_{200} \geq 2$ as c_0 . However, it is pointed out recently that the number of high p_T jets increases significantly if matrix element (ME) corrections are included [31]. On the other hand, \not{E}_T cut does not affected by ME corrections. The $c^{(3)}$ cut reduces background efficiently.

F. Summary of the cuts

It is important to reduce the background from $\tilde{g}\tilde{q}$ production to measure $\tilde{q}_L\tilde{q}_L$ production cross section using SS2l events. We give a systematic procedure to separate \tilde{g} and \tilde{q} based on

number of jet	all	$n_{100} \geq 2$			$n_{200} \geq 2$		
$\cancel{E}_T, M_{\text{eff}}$ cut	all	$c^{(1)}$	$c^{(2)}$	$c^{(3)}$	$c^{(1)}$	$c^{(2)}$	$c^{(3)}$
$N(l^+l^+ \text{ from } \tilde{q}\tilde{q}; c_0)$	356	216	211	197	162	159	150
$N(l^+l^+ \text{ from } \tilde{g}\tilde{q}; c_0)$	333	169	169	161	122	122	119
$N(l^+l^+ \text{ from } \tilde{q}\tilde{q}; c_5)$	*	72	67	61	59	56	52
$N(l^+l^+ \text{ from } \tilde{g}\tilde{q}; c_5)$	*	2	2	2	2	2	2
$N(l^+l^+; c_5)/N(l^+l^+; c_0)$ for $\tilde{q}\tilde{q}$	*	0.333	0.318	0.310	0.364	0.352	0.347
$N(l^+l^+; c_5)/N(l^+l^+; c_0)$ for $\tilde{g}\tilde{q}$	*	0.012	0.012	0.012	0.016	0.016	0.017
$N(l^-l^- \text{ from } \tilde{q}\tilde{q}; c_0)$	84	55	54	50	38	37	36
$N(l^-l^- \text{ from } \tilde{g}\tilde{q}; c_0)$	131	63	60	56	47	47	46
$N(l^-l^- \text{ from } \tilde{q}\tilde{q}; c_5)$	*	16	15	15	14	13	13
$N(l^-l^- \text{ from } \tilde{g}\tilde{q}; c_5)$	*	1	1	1	1	1	1
$N(l^-l^-; c_5)/N(l^-l^-; c_0)$ for $\tilde{q}\tilde{q}$	*	0.291	0.278	0.300	0.368	0.351	0.361
$N(l^-l^-; c_5)/N(l^-l^-; c_0)$ for $\tilde{g}\tilde{q}$	*	0.016	0.017	0.018	0.021	0.021	0.022

TABLE IX: Numbers of SS2 l events at Point D after various c_0 cuts for 307.06 fb $^{-1}$

the number of jets in a hemisphere, and demonstrate that it works well to separate $\tilde{q}_L\tilde{q}_L$ from $\tilde{g}\tilde{q}$ for our model points. The hemisphere cut should work as far as $m_{\tilde{g}} - m_{\tilde{q}}$ is sufficiently large so that a jet from the decay $\tilde{g} \rightarrow \tilde{q}q$ is detectable.

Using the cut on the number of jets in a hemisphere and b -jet veto, SS2 l events from $\tilde{g}\tilde{q}$ production are reduced by more than 95% while SS2 l events from $\tilde{q}_L\tilde{q}_L$ are left by more than 30% at our model points. Moreover, these efficiencies depend only weakly on the basic cut of \cancel{E}_T and M_{eff} .

Evidence of squark pair production can be seen in the ratio of the events before and after the hemisphere cuts, because it is significantly different from that of $\tilde{g}\tilde{q}$ production. At Point B, the ratio $N(l^+l^+; c_5)/N(l^+l^+; c_0)$ is 0.171 with the statistical error ~ 0.01 . If $\tilde{q}\tilde{q}$ production does not occur, $N(l^+l^+; c_0)$ becomes 1559, $N(l^+l^+; c_5)$ becomes 80 and the ratio becomes 0.051 with statistical error ~ 0.006 . Actually, there are various sources of systematic errors such as uncertainties on the PDF, NNLO corrections and so on. The total systematic error is 14%, if the uncertainties from squark and gluino mass errors cancel in the ratio and ignore the errors on branching ratios. However we think there is enough margin to identify

$\tilde{q}_L\tilde{q}_L$ production if careful analyses are done at LHC.

IV. COMPARISON OF OTHER MODELS WITH THE MSSM

A. The model with an extended gluino sector

The model with an extended gluino sector has been discussed in the section 2.2. In this model, a gluino acquires a Dirac mass term with an adjoint fermion \tilde{a} . As the majorana gluino mass parameter decreases from the MSSM value for the same gluino mass, the total SUSY production cross section decreases. Especially $\sigma(\tilde{q}_L\tilde{q}_L)$ decreases more rapidly than $\sigma(\tilde{g}\tilde{q}_L)$ when the majorana gluino mass parameter is reduced. Then, SS2 l events from $\tilde{q}_L\tilde{q}_L$ decrease more than that from $\tilde{g}\tilde{q}_L$. Figure 10a shows $N(l^\pm l^\pm; c_0)$ as a function of the majorana gluino mass. Here, we set the mass spectrum of this model as that of Point B and $m_{\tilde{g}_1} = m_{\tilde{g}}$ and $m_{\tilde{g}_2} = -3000\text{ GeV}$, and branching ratios and efficiencies of cuts are the same as in the previous section. Moreover, we simplify our calculation by assuming that all $l^\pm l^\pm$ events from $\tilde{q}\tilde{q}$ production occur from $\tilde{q}_L^+\tilde{q}_L^+$ productions (see Appendix A 3) and that non- \tilde{g} , non- \tilde{q}_L contribution does not depend on m_g . We show $N(l^+l^+; c_0)$ in a bold solid line, $N(l^-l^-; c_0)$ in a bold dashed line, $N(l^+l^+ \text{ from } \tilde{q}\tilde{q}; c_0)$ in a thin solid line and $N(l^-l^- \text{ from } \tilde{q}\tilde{q}; c_0)$ in a thin dashed line.

Figure 10b shows $N(l^\pm l^\pm; c_5)$. SS2 l events from $\tilde{q}_L^+\tilde{q}_L^+$ are dominant in the total SS2 l events after c_5 cut, and that the dependency on the majorana gluino mass of the total SS2 l events are nearly the same as the $\sigma(\tilde{q}_L\tilde{q}_L)$ dependence shown in Figure 7. On the other hand, $\tilde{g}\tilde{q}$ contribution is dominant in Figure 10a.

We show the $\pm 1\sigma$ statistical error for the MSSM limits with a dark gray zone. The absolute numbers of SS2 l events after the cut c_0, c_5 depend on various parameters, acceptance and so on. We assume the total uncertainty is 17% as discussed in the previous section. This is also shown in Figure 10 with a light gray zone.

The $N(l^+l^+(l^-l^-); c_0)$ shows more than 17% deviation from the MSSM in case of $m_g \leq 606\text{ GeV}$ ($m_g \leq 459\text{ GeV}$). This means $m_D \geq 1262\text{ GeV}$ ($m_D \geq 1427\text{ GeV}$). It is $m_g \leq 936\text{ GeV}$ ($m_g \leq 730\text{ GeV}$) for $N(l^+l^+(l^-l^-); c_5)$. This means $m_D \geq 664\text{ GeV}$ ($m_D \geq 1089\text{ GeV}$).

As discussed in the previous section, the uncertainties on the leptonic branching ra-

tios, PDF, QCD NNLO corrections and squark mass errors partly cancel by taking the ratio $N(l^+l^+; c_5)/N(l^+l^+; c_0)$. Roughly speaking, $N(l^\pm l^\pm; c_5)/N(l^\pm l^\pm; c_0)$ depends linearly on $\sigma(\tilde{q}_L^+\tilde{q}_L^+)/\sigma(\tilde{q}\tilde{q}_L)$. In this model, the ratio $\sigma(\tilde{q}_L^\pm\tilde{q}_L^\pm)/\sigma(\tilde{q}\tilde{q}_L^\pm)$ decreases as the majorana gluino mass decreases from the MSSM value. The ratios $N(l^\pm l^\pm; c_5)/N(l^\pm l^\pm; c_0)$ as the function of the majorana gluino mass are plotted for Point A~D in Figure 11a~d. We show only the statistical error of $\pm 1\sigma$ in the MSSM limit for 3×10^5 events with a gray zone. For example, the ratio $N(l^\pm l^\pm; c_5)/N(l^\pm l^\pm; c_0)$ has the statistically significant difference from Point B for $m_g \leq 850$ GeV at the 1σ level. Because of the $\sigma(\tilde{q}^-\tilde{q}^-) \ll \sigma(\tilde{q}^+\tilde{q}^+)$ the sensitivity to l^-l^- is worse.

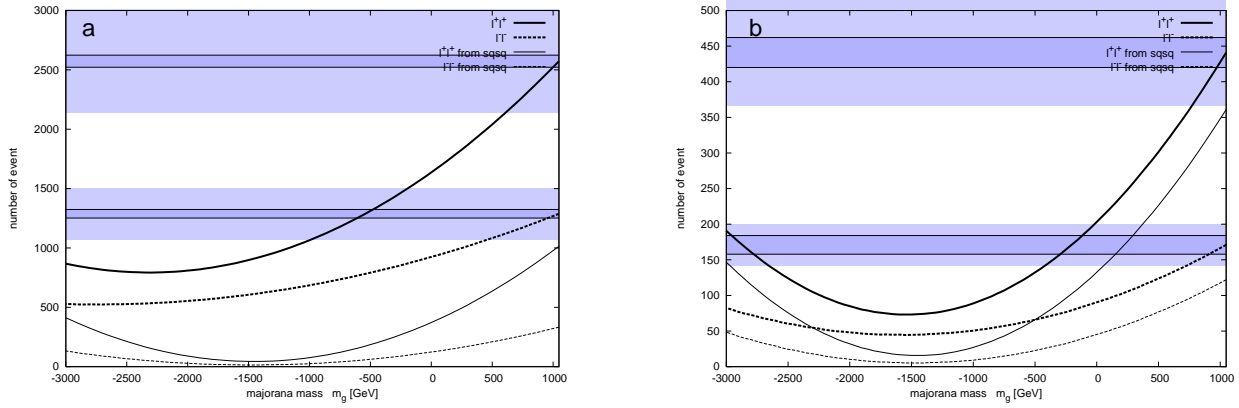


FIG. 10: Number of SS2 l events as a function of the gluino majorana mass at Point B a) after the cut c_0 , b) after the cut c_5 . Dark gray zones show 1σ statistical errors for 3×10^5 events. Light gray zones show 17% errors.

B. The Littlest Higgs model with T-parity

We now consider the case where the \cancel{E}_T signature arises from decays of quark partner q_- in the LHT model. The q_- has the similar decay pattern to the \tilde{q} . Indeed, the leptonic branching ratio of q_-^+ is $\sim 15\%$, which is almost the same as that of \tilde{q}^+ at Point C and D. The acceptance should be similar to that of the MSSM, because the acceptance depends on the decay kinematics, namely on the mass difference between \tilde{q} or q_- mass and the lightest R-odd or T-odd particle.

While the collider signal is similar to that of $\tilde{q}\tilde{q}$ production in the MSSM, the LHT model predicts different production cross sections from that of the MSSM. The cross section

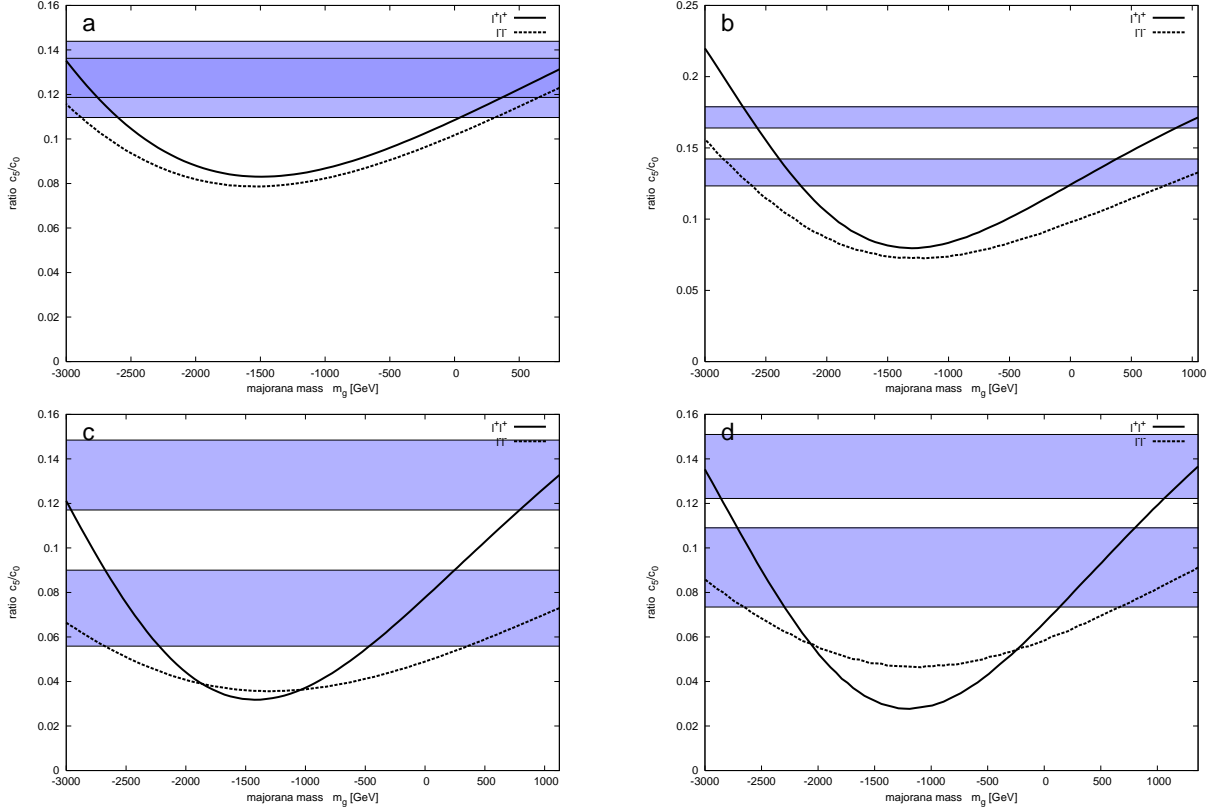


FIG. 11: $N(c_5)/N(c_0)$ dependence on the majorana gluino mass m_g at a) Point A, b) Point B, c) Point C and d) Point D. Gray zones show 1σ statistical errors for 3×10^5 events.

$\sigma(q_-^+ q_-^+)$ is 0.70 pb and $\sigma(q_-^- q_-^-)$ is 0.15 pb for $M_{q_-} \sim 800$ GeV. On the other hand, $\sigma(\tilde{q}_L^+ \tilde{q}_L^+)$ is 0.13 pb and $\sigma(\tilde{q}_L^- \tilde{q}_L^-)$ is 0.037 pb at Point C ($m_{\tilde{q}} \sim 800$ GeV). For $M_{q_-} = 1000$ GeV, $\sigma(q_-^+ q_-^+)$ is 0.22 pb and $\sigma(q_-^- q_-^-)$ is 0.045 pb, while the $\sigma(\tilde{q}_L^+ \tilde{q}_L^+)$ is 0.049 pb and $\sigma(\tilde{q}_L^- \tilde{q}_L^-)$ is 0.012 pb at Point D ($m_{\tilde{q}} \sim 1000$ GeV). The $\sigma(q_-^\pm q_-^\pm)$ is about 4~5 times larger than $\sigma(\tilde{q}_L^\pm \tilde{q}_L^\pm)$ at each point. Note that $\sigma(\tilde{q}_L \tilde{q}_L)$ is always significantly smaller than $\sigma(q_- q_-)$ of the LHT model no matter how heavy or light the \tilde{q} is. Moreover, there is no \tilde{g} productions in the LHT model. If the excess of the production cross section is established and the existence of a light gluino is excluded, we can claim the LHT signature is observed.

At Point C, $N(l^+l^+; c_0) = 467$, $N(l^-l^-; c_0) = 233$, $N(l^+l^+; c_5) = 62$ and $N(l^-l^-; c_5) = 17$ for the integrated luminosity 86 fb^{-1} . To study the $N(l^+l^+)$ or $N(l^-l^-)$, we need to simulate all LHT production processes, which is beyond the scope of this paper. We assume the number of the signal from $q_- q_-$ production process is the number of the signal from $\tilde{q}\tilde{q}$ production process scaled by the ratio of cross sections $\sigma(q_- q_-)/\sigma(\tilde{q}_L \tilde{q}_L)$, and the other production processes are ignored for simplicity. We expect $N(l^+l^+; c_0) \sim 816$, $N(l^-l^-; c_0) \sim$

162, $N(l^+l^+; c_5) \sim 302$ and $N(l^-l^-; c_5) \sim 49$ in the LHT model of $M_{q_-} \sim 800$ GeV for the same integrated luminosity.

At Point D, we find $N(l^+l^+; c_0) = 571$, $N(l^-l^-; c_0) = 263$, $N(l^+l^+; c_5) = 78$ and $N(l^-l^-; c_5) = 24$ for the integrated luminosity 307fb^{-1} . We expect $N(l^+l^+; c_0) \sim 962$, $N(l^-l^-; c_0) \sim 210$, $N(l^+l^+; c_5) \sim 321$ and $N(l^-l^-; c_5) \sim 61$ in the LHT model of $M_{q_-} \sim 1000$ GeV for the same integrated luminosity. We can see in the LHT models, $N(l^+l^+; c_0) : N(l^-l^-; c_0)$ would be about 4:1. This is different from the cases at the MSSM models Point C and D.

If there is no particle production except q_- 's the ratio $N(l^+l^+; c_5)/N(l^+l^+; c_0)$ is expected around 0.37 in the LHT model of $M_{q_-} \sim 800$ GeV, which is larger than the value at Point C (0.133). The ratio $N(l^+l^+; c_5)/N(l^+l^+; c_0)$ is expected around 0.33 for $M_q = 1000$ GeV, and the value is larger than that at Point D (0.137).

Finally we comment on the case where \tilde{q} and \tilde{g} is highly degenerate so that we cannot detect the jets from $\tilde{g} \rightarrow \tilde{q}\tilde{q}$ decay by hemisphere analysis. Note that $\sigma(\tilde{g}\tilde{q}) \gg \sigma(\tilde{q}\tilde{q})$, therefore rate of the SS2 l events could be as large as the LHT prediction. However, even in the case, $N(l^+l^+; c_0) : N(l^-l^-; c_0)$ in the MSSM is $\sim 2:1$ and cannot be 4:1 because there are $\tilde{g}\tilde{q}$ and $\tilde{g}\tilde{g}$ contributions.

V. CONCLUSION

The information on the fundamental Lagrangian of SUSY model can be extracted from each SUSY production process at LHC. For example, $\tilde{q}_L\tilde{q}_L$ production process cannot occur without majorana gluino mass, because chirality flip is required. Thus majorana nature of gluino mass can be extracted from this process.

The process can be investigated using the SS2 l events because $\mathcal{BR}(\tilde{q}_L^\pm \rightarrow l^\pm X) \gg \mathcal{BR}(\tilde{q}_L^\pm \rightarrow l^\mp X)$. At LHC, however, mixed productions with other sparticles \tilde{g} , \tilde{q} , etc. make it difficult to interpret the signal. Especially, the $\tilde{g}\tilde{q}$ production also contribute to the SS2 l channel.

In this paper, we have discussed the systematic method to separate the production modes. When we measure the $\sigma(\tilde{q}_L\tilde{q}_L \rightarrow l^\pm l^\pm + X)$ in the MSSM, we suffer from the problematic background of $\tilde{g}\tilde{q}_L$ productions. We have proposed a new method based on a hemisphere analysis as a solution of this problem. In the hemisphere analysis, we assign high p_T objects

into two hemispheres, where each hemisphere contains high p_T objects from the same parent particle with high probability. Then we require the cut where there is only one jet with $p_T > 50 \text{ GeV}$ in a hemisphere. For the sample after some basic cuts, 30~40% for $\tilde{q}_L \tilde{q}_L$ and 1~3% for $\tilde{g} \tilde{q}_L$ remain after the hemisphere cut. Therefore we can obtain $\text{SS2}l$ events with enhanced $\tilde{q}_L \tilde{q}_L$ contribution, which may be used to an estimation of the $\sigma(\tilde{q}_L \tilde{q}_L)$.

We have also discussed two models which have similar collider signals to the MSSM but the relevant production cross sections are dramatically different.

One of the models is the MSSM with an extended gluino sector, where the gluino can have a Dirac mass with an adjoint fermion \tilde{a} . The $\sigma(\tilde{q}_L \tilde{q}_L)$ is sensitive to the fraction of majorana mass terms in the gluino mass. In case where the gluino is pure Dirac, $\tilde{q}_L \tilde{q}_L$ production cross section becomes zero.

We have applied our analysis to the model points with an extended gluino sector which has the same mass spectra of some MSSM model points except for an additional heavy adjoint particle. We estimate $\text{SS2}l$ events as the function of the majorana gluino mass, and estimate the sensitivity to the Dirac gluino mass. We take only the statistical error into account and assume that masses of the squarks and the branching ratios are known. We find that the ratio $\sigma(\tilde{q}_L^+ \tilde{q}_L^+)/\sigma(\tilde{g} \tilde{q}_L^+)$ that can be estimated from the acceptance under the hemisphere cut is useful because this quantity should be less sensitive to the error on the parameters and the acceptance and uncertainties of the PDF and QCD corrections.

We have also considered the LHT model. In this model, a set of T-odd partners is introduced to the SM matters and the EW gauge bosons. The quark partner production cross section $\sigma(q_- q_-)$ is 4~5 times as large as the production cross section $\sigma(\tilde{q}_L \tilde{q}_L)$ in the MSSM. The q_- and \tilde{q} have similar decay patterns and branching ratios. Thus, the number of $\text{SS2}l$ events from $q_- q_-$ productions in the LHT model is expected 4~5 times larger if patterns of the mass spectra are the same. Moreover, the LHT model has no process corresponding to the process $\tilde{g} \tilde{q}$ nor $\tilde{g} \tilde{g}$ production in the MSSM. Excluding the case where the gluino decays into squarks from $\tilde{g} \tilde{q}$ productions mimic $\tilde{q} \tilde{q}$ productions is important to identify the LHT model. This can be done by investigating $N(l^+ l^+)/N(l^- l^-)$.

It is generally important to measure the production cross sections of sparticles separately to verify the MSSM and distinguish various models. In this paper, we develop a method to identify gluino and squark production separately for $\text{SS2}l$ channel. The method is based on the cuts on the kinematical configuration of the jets and can be applied to the other models.

More development is needed for the model independent study of physics beyond the SM.

Acknowledgement

This work is supported in part by the Grant-in-Aid for Science Research, Ministry of Education, Culture, Sports, Science and Technology, Japan (No.16081207, 18340060 for M.M.N.).

APPENDIX A: APPENDIX

1. Mass spectra at our model points

We show mass spectra for the selected model points which have been analyzed. They are calculated by ISAJET 7.72. They are all mSUGRA mass spectra except that gluino masses of Point C and D are 300 GeV larger than mSUGRA predictions.

mass parameter	Point A	Point B	Point C	Point D	SPS1a
m_0	100	100	370	400	100
$m_{\frac{1}{2}}$	340	450	340	450	250
A_0	0	0	0	0	-100
$\tan \beta$	10	10	10	10	10
sign μ	+	+	+	+	+

particle	Point A	Point B	Point C	Point D	SPS1a
\tilde{g}	809.86	1047.83	1123.23	1360.22	595.19
\tilde{d}_L	741.58	954.53	812.70	1021.11	543.04
\tilde{u}_L	737.25	951.16	808.67	1017.91	537.25
\tilde{d}_R	712.94	916.48	786.98	986.09	520.14
\tilde{u}_R	714.56	919.51	787.79	988.10	520.45
\tilde{b}_1	683.97	883.16	731.10	928.37	491.92
\tilde{t}_1	559.18	734.57	585.39	804.20	379.14
\tilde{b}_2	708.33	909.55	776.58	973.96	524.58
\tilde{t}_2	738.66	929.69	780.92	946.08	574.64
\tilde{e}_L	256.36	324.47	437.13	503.38	202.12
\tilde{e}_R	168.27	201.70	393.09	435.59	143.00
$\tilde{\nu}_e$	243.67	314.44	429.70	496.84	186.00
$\tilde{\tau}_1$	160.79	194.28	387.18	429.40	133.39
$\tilde{\tau}_2$	258.50	325.66	437.28	503.05	206.02
$\tilde{\nu}_\tau$	242.89	313.50	428.00	495.00	185.06
$\tilde{\chi}_1^0$	132.74	179.11	133.95	180.54	96.05
$\tilde{\chi}_2^0$	253.87	345.39	256.39	348.15	176.80
$\tilde{\chi}_3^0$	-448.66	-575.60	-451.46	-577.05	-358.82
$\tilde{\chi}_4^0$	467.28	591.37	470.52	592.66	377.84
$\tilde{\chi}_1^+$	254.13	345.95	256.71	348.72	176.37
$\tilde{\chi}_2^+$	466.48	590.74	469.74	592.56	378.26

TABLE X: Mass spectra of sparticles for the selected model points

2. Branching ratios at our model points

We also show the branching ratios of the selected points. They are also calculated by ISAJET. Squarks mainly decay into charginos $\tilde{\chi}^\pm$ and the second lightest neutralino $\tilde{\chi}_2^0$ at each point. Note that, at Point C and D, $\tilde{\chi}_2^0$ does not decay into sleptons. On the other hand, at Point A, B and SPS1a, $\tilde{\chi}_2^0$ decays into $\tilde{\chi}_1^0 l^+ l^-$ or $\tilde{\chi}_1^0 \tau^+ \tau^-$.

mode	BR(%)					mode	BR(%)					
	A	B	C	D	SPS1a		A	B	C	D	SPS1a	
$\tilde{g} \rightarrow \tilde{q}_L^+ q$	11	10	14	13	12	$\tilde{t}_1 \rightarrow \tilde{\chi}_1^+ b$	49	39	43	6.9	73	
	$\rightarrow \tilde{q}_L^- q$	11	10	14	13	12	$\rightarrow \tilde{\chi}_2^+ b$	13	21	20	41	0
	$\rightarrow \tilde{q}_R q$	38	36	32	32	41	$\rightarrow \tilde{\chi}_1^0 t$	22	26	22	24	18
	$\rightarrow \tilde{t}_1 \bar{t} (\tilde{t}_1^* t)$	7.1	9.6	5.3	7	4.1	$\rightarrow \tilde{\chi}_2^0 t$	15	14	14	3	9.5
	$\rightarrow \tilde{b}_1 \bar{b} (\tilde{b}_1^* b)$	7.7	6.9	5.1	5	8.9	$\rightarrow \tilde{\chi}_3^0 t$	0	0	0	15	0
	$\rightarrow \tilde{b}_2 \bar{b} (\tilde{b}_2^* b)$	5.5	5.2	4.2	4.2	4.9	$\rightarrow \tilde{\chi}_4^0 t$	0	0	0	10	0
	$\rightarrow \tilde{t}_2 \bar{t} (\tilde{t}_2^* t)$	0	0	5.4	4.5	0	$\tilde{t}_2 \rightarrow \tilde{\chi}_1^+ b$	23	25	22	41	19
$\tilde{u}_L \rightarrow \tilde{\chi}_1^+ d$	65	65	64	64	65	$\rightarrow \tilde{\chi}_2^+ b$	16	12	1.5	2.8	22	
	$\rightarrow \tilde{\chi}_2^+ d$	1.6	1.4	1.9	1.5	1.2	$\rightarrow \tilde{\chi}_2^0 t$	9.7	11	9.5	18	7.6
	$\rightarrow \tilde{\chi}_1^0 u$	0	1.1	0	1	0.6	$\rightarrow \tilde{\chi}_3^0 t$	8.5	10	11	18	3.7
	$\rightarrow \tilde{\chi}_2^0 u$	32	32	32	32	32	$\rightarrow \tilde{\chi}_4^0 t$	24	23	25	19	18
	$\rightarrow \tilde{\chi}_4^0 u$	1.2	0.9	1.4	1.1	1.0	$\rightarrow \tilde{t}_1 X$	17	17	17	0	27
$\tilde{d}_L \rightarrow \tilde{\chi}_1^- u$	61	62	60	62	61	$\tilde{\chi}_2^- \rightarrow \tilde{\chi}_1^- X$	44	48	54	55	41	
	$\rightarrow \tilde{\chi}_2^- u$	4.4	3.3	5	3.6	4.1	$\rightarrow \tilde{\chi}_1^0 W^-$	37	38	45	42	36
	$\rightarrow \tilde{\chi}_1^0 d$	2	1.8	1.9	1.7	2.4	$\rightarrow l^- X$	12	6.7	0	0	14
	$\rightarrow \tilde{\chi}_2^0 d$	31	32	31	31	31	$\rightarrow \tau^- X$	7.2	5.4	0	0	6.6
	$\rightarrow \tilde{\chi}_4^0 d$	1.6	1.2	1.9	1.4	1.4	$\tilde{\chi}_1^- \rightarrow \tilde{\chi}_1^0 W^-$	21	7.7	100	100	1.1
$\tilde{b}_1 \rightarrow \tilde{\chi}_1^- t$	38	36	33	38	43	$\rightarrow \tilde{\chi}_1^0 l^- \bar{\nu}_l$	24	54	0	0	0.4	
	$\rightarrow \tilde{\chi}_2^- t$	24	28	31	37	0	$\rightarrow \tilde{\chi}_1^0 \tau^- \bar{\nu}_\tau$	54	38	0	0	98
	$\rightarrow W^- \tilde{t}_1$	10	12	12	0	14	$\tilde{\chi}_2^0 \rightarrow \tilde{\chi}_1^0 X$	45	55	100	100	0.8
	$\rightarrow \tilde{\chi}_2^0 b$	24	21	20	22	36	$\rightarrow \tilde{\chi}_1^0 l^+ l^-$	7.6	18	0	0	13
$\tilde{b}_2 \rightarrow \tilde{\chi}_1^- t$	15	14	4.9	4.4	21	$\rightarrow \tilde{\chi}_1^0 \tau^+ \tau^-$	46	20	0	0	87	
	$\rightarrow \tilde{\chi}_2^- t$	34	35	39	41	0	$\tilde{\chi}_3^0 \rightarrow \tilde{\chi}_1^0 X$	14	13	14	14	13
	$\rightarrow W^- \tilde{t}_1$	13	13	13	0	35	$\rightarrow \tilde{\chi}_2^0 X$	24	26	25	27	23
	$\rightarrow \tilde{\chi}_1^0 b$	19	21	23	31	15	$\rightarrow \tilde{\chi}_1^\pm W^\mp$	29	29	30	30	60
	$\rightarrow \tilde{\chi}_2^0 b$	9.6	8.3	3	2.5	17	$\tilde{\chi}_4^0 \rightarrow \tilde{\chi}_1^0 X$	21	19	12	13	8.5
	$\rightarrow \tilde{\chi}_3^0 b$	3.7	3.5	7.9	9.4	5.4	$\rightarrow \tilde{\chi}_2^0 X$	18	22	22	25	15
	$\rightarrow \tilde{\chi}_4^0 b$	5.6	5.2	9.6	11	7.4	$\rightarrow \tilde{\chi}_1^\pm W^\mp$	26	26	32	30	52

TABLE XI: Branching ratios of sparticles for our model points: here, X means some SM particles.

3. Dominant processes contributing to SS2*l* events

Here, we show the numbers of SS2*l* events from each production process at Point B. Note that SS2*l* ($l^\pm l^\pm$) signals come from not only $\tilde{q}_L^\pm \tilde{q}_L^\pm$ productions but also $\tilde{q}_L^+ \tilde{q}_L^-$ (mainly $u_L d_L$) productions. For $l^+ l^+$ events, they are about 6% of total $l^+ l^+$ events from $\tilde{q} \tilde{q}$ productions. The $l^+ l^+$ events from $\tilde{q}_L \tilde{q}_L^*$ productions are 10% of total $l^+ l^+$ events from $\tilde{q} \tilde{q}$ productions.

Point B	all	c_0	c_1	c_2	c_3	c_4	c_5	ratio
l^+l^+	$\tilde{q}\tilde{q}$	1479	1014	1001	894	363	883	361 0.356
	$\tilde{u}_L\tilde{u}_L$	1161	788	778	701	291	692	289 0.367
	$\tilde{u}_L\tilde{c}_L$	95	68	68	58	22	58	22 0.324
	$\tilde{u}_L\tilde{d}_L$	84	58	56	51	17	50	17 0.293
	$\tilde{u}_L\tilde{d}_L^*$	90	62	61	54	19	53	19 0.306
	$\tilde{u}_L\tilde{s}_L^*$	48	37	37	29	13	29	13 0.351
l^+l^+	$\tilde{g}\tilde{q}$	1765	1098	433	613	52	279	36 0.033
	$\tilde{g}\tilde{u}_L$	1581	974	388	538	41	252	30 0.031
	$\tilde{g}\tilde{c}_L$	22	18	8	8	2	3	1 0.056
	$\tilde{g}\tilde{d}_L$	32	22	8	11	2	5	1 0.045
	$\tilde{g}\tilde{d}_L^*$	78	53	17	38	6	12	3 0.057
	$\tilde{g}\tilde{s}_L^*$	39	22	9	13	0	6	0 0

Point B	all	c_0	c_1	c_2	c_3	c_4	c_5	ratio
l^-l^-	$\tilde{q}\tilde{q}$	519	333	323	293	123	285	122 0.366
	$\tilde{d}_L\tilde{d}_L$	280	188	181	164	74	159	73 0.388
	$\tilde{d}_L\tilde{s}_L$	87	62	61	56	31	55	31 0.5
	$\tilde{u}_L\tilde{d}_L$	106	67	65	57	16	55	16 0.239
	$\tilde{d}_L\tilde{u}_L^*$	20	7	7	7	0	7	0 0
	$\tilde{d}_L\tilde{c}_L^*$	10	7	7	7	1	7	1 0.143
l^-l^-	$\tilde{g}\tilde{q}$	881	553	241	310	23	172	15 0.027
	$\tilde{g}\tilde{d}_L$	615	396	184	232	21	132	14 0.035
	$\tilde{g}\tilde{s}_L$	30	18	8	9	0	5	0 0
	$\tilde{g}\tilde{u}_L$	135	75	23	40	2	17	1 0.013
	$\tilde{g}\tilde{u}_L^*$	67	43	19	21	0	13	0 0
	$\tilde{g}\tilde{c}_L^*$	20	12	4	6	0	3	0 0

TABLE XII: Contributions from each production process to SS2 l events at Point B.

[1] D. N. Spergel *et al.* [WMAP Collaboration], *Astrophys. J. Suppl.* **148**, 175 (2003) arXiv:astro-ph/0302209.
 D. N. Spergel *et al.*, arXiv:astro-ph/0603449.

[2] ALTAS Technical Design Report, CERN/LHCC-99-15, ATL-PHYS-98-131 (1998).

[3] CMS Physics Technical Design Report, CERN/LHCC 2006-001, CMS TDR 8.1 02 February 2006.

[4] I. Antoniadis, *Phys. Lett. B* **246**, 377 (1990).
 T. Appelquist, H. C. Cheng and B. A. Dobrescu, *Phys. Rev. D* **64**, 035002 (2001) [arXiv:hep-ph/0012100].

[5] J. Hubisz and P. Meade, *Phys. Rev. D* **71**, 035016 (2005) [arXiv:hep-ph/0411264].

[6] A. Freitas and P. Z. Skands, *JHEP* **0609**, 043 (2006) [arXiv:hep-ph/0606121].

[7] P. J. Fox, A. E. Nelson and N. Weiner, *JHEP* **0208**, 035 (2002) [arXiv:hep-ph/0206096].

[8] Z. Chacko, P. J. Fox and H. Murayama, *Nucl. Phys. B* **706**, 53 (2005) [arXiv:hep-ph/0406142].

[9] L. M. Carpenter, P. J. Fox and D. E. Kaplan, arXiv:hep-ph/0503093.

[10] J. Hisano, M. Nagai, T. Naganawa and M. Senami, *Phys. Lett. B* **644**, 256 (2007) [arXiv:hep-ph/0610383].

[11] A. Belyaev, C. R. Chen, K. Tobe and C. P. Yuan, *Phys. Rev. D* **74**, 115020 (2006) [arXiv:hep-ph/0609179].

[12] F. Moortgat and L. Pape, CMS Physics TDR Chapter 13.4, p.400-403, CERN/LHCC/2006-021 (26 June 2006).

[13] S. Kretzer, H. L. Lai, F. I. Olness and W. K. Tung, *Phys. Rev. D* **69**, 114005 (2004) [arXiv:hep-ph/0307022].

[14] G. Weiglein *et al.* [LHC/LC Study Group], *Phys. Rept.* **426**, 47 (2006) [arXiv:hep-ph/0410364].

[15] B. C. Allanach *et al.*, in *Proc. of the APS/DPF/DPB Summer Study on the Future of Particle Physics (Snowmass 2001)* ed. N. Graf, *In the Proceedings of APS / DPF / DPB Summer Study on the Future of Particle Physics (Snowmass 2001)*, Snowmass, Colorado, 30 Jun - 21 Jul 2001, pp P125 [arXiv:hep-ph/0202233].

[16] H. Baer, F. E. Paige, S. D. Protopopescu and X. Tata, arXiv:hep-ph/9305342.

- [17] F. E. Paige, S. D. Protopopescu, H. Baer and X. Tata, arXiv:hep-ph/0312045.
- [18] G. Corcella *et al.*, arXiv:hep-ph/0210213.
- [19] N. Arkani-Hamed, A. G. Cohen, E. Katz and A. E. Nelson, JHEP **0207**, 034 (2002) [arXiv:hep-ph/0206021].
- [20] C. Csaki, J. Hubisz, G. D. Kribs, P. Meade and J. Terning, Phys. Rev. D **67**, 115002 (2003) [arXiv:hep-ph/0211124].
- [21] J. L. Hewett, F. J. Petriello and T. G. Rizzo, JHEP **0310**, 062 (2003) [arXiv:hep-ph/0211218].
- [22] E. Richter-Was, arXiv:hep-ph/0207355.
- [23] I. Hinchliffe, F. E. Paige, M. D. Shapiro, J. Soderqvist and W. Yao, Phys. Rev. D **55**, 5520 (1997) [arXiv:hep-ph/9610544].
- [24] H. Bachacou, I. Hinchliffe and F. E. Paige, Phys. Rev. D **62**, 015009 (2000) [arXiv:hep-ph/9907518].
- [25] I. Hinchliffe and F. E. Paige, Phys. Rev. D **61**, 095011 (2000) [arXiv:hep-ph/9907519].
- [26] I. Hinchliffe and F. E. Paige, Phys. Rev. D **60**, 095002 (1999) [arXiv:hep-ph/9812233].
- [27] J. Hisano, K. Kawagoe and M. M. Nojiri, Phys. Rev. D **68**, 035007 (2003) [arXiv:hep-ph/0304214].
- [28] K. Kawagoe, M. M. Nojiri and G. Polesello, Phys. Rev. D **71**, 035008 (2005) [arXiv:hep-ph/0410160].
- [29] W. Beenakker, R. Höpker, M. Spira and P. M. Zerwas, Nucl. Phys. B **492**, 51 (1997); T. Plehn, *Prospino 2.0* [pheno.physics.wisc.edu/~plehn/prospino/prospino.html].
- [30] S. Matsumoto, M. M. Nojiri and D. Nomura, arXiv:hep-ph/0612249.
- [31] S. Asai, talk in 4th TEV4LHC, Oct 20 -22, 2005 at FermiLab.
<http://conferences.fnal.gov/tev4lhc/>